SANDIA REPORT
SAND2000-3157
Unlimited Release
Printed March 2001

Thin Film Models of Magnesium Orthovanadate Catalysts for Oxidative Dehydrogenation

Allen G. Sault, Jason E. Mudd, James E. Miller, Judith A. Ruffner, Mark A. Rodriquez, and Ralph G. Tissot, Jr.

Prepared by
Sandia National Laboratories
Albuquerque, New Mexico 87185 and Livermore, California 94550

Sandia is a multiprogram laboratory operated by Sandia Corporation, a Lockheed Martin Company, for the United States Department of Energy under Contract DE-AC04-94AL85000.

Issued by Sandia National Laboratories, operated for the United States Department of Energy by Sandia Corporation.

Available to DOE and DOE contractors from
U.S. Department of Energy
Office of Scientific and Technical Information
P.O. Box 62
Oak Ridge, TN 37831

Telephone: (865)576-8401
Facsimile: (865)576-5728
E-Mail: reports@adonis.osti.gov
Online ordering: http://www.doe.gov/bridge

Available to the public from
U.S. Department of Commerce
National Technical Information Service
5285 Port Royal Rd
Springfield, VA 22161

Telephone: (800)553-6847
Facsimile: (703)605-6900
E-Mail: orders@ntis.fedworld.gov
Online order: http://www.ntis.gov/ordering.htm

SAND2000-3157
Unlimited Release
Printed March 2001

Thin Film Models of Magnesium Orthovanadate Catalysts for Oxidative Dehydrogenation

Allen G. Sault, Jason E. Mudd, and James E. Miller
Catalytic and Porous Materials Department

Judith A. Ruffner
Electronic & Optical Materials Department

Mark A. Rodriguez and Ralph G. Tissot, Jr.
Materials Characterization Department

Sandia National Laboratories
P.O. Box 5800
Albuquerque, New Mexico 87185-1349

Abstract

Magnesium vanadates are potentially important catalytic materials for the conversion of alkanes to alkenes *via* oxidative dehydrogenation. However, little is known about the active sites at which the catalytic reactions take place. It may be possible to obtain a significant increase in the catalytic efficiency if the effects of certain material properties on the surface reactions could be quantified and optimized through the use of appropriate preparation techniques. Given that surface reactivity is often dependent upon surface structure and that the atomic level structure of the active sites in these catalysts is virtually unknown, we desire thin film samples consisting of a single magnesium vanadate phase and a well defined crystallographic orientation in order to reduce complexity and simplify the study of active sites. This report describes the use of reactive RF sputter deposition to fabricate very highly oriented, stoichiometric $Mg_3(VO_4)_2$ thin films, and subsequent studies of the reactivity of these films under reaction conditions typically found during oxidative dehydrogenation. We demonstrate that the synthesis methods employed do in fact result in stoichiometric films with the desired crystallographic orientation, and that the chemical behavior of the films closely approximates that of bulk, high surface area $Mg_3(VO_4)_2$ powders. We further use these films to demonstrate the effects of oxygen vacancies on chemical behavior, demonstrate that surface composition can vary significantly under reaction conditions, and obtain the first evidence for structure sensitivity in $Mg_3(VO_4)_2$ catalysts.

Acknowledgements

We gratefully acknowledge Dr. John A. Shelnutt of Sandia National Laboratories for his assistance in modeling the $Mg_3(VO_4)_2$ crystal structure. The authors also thank Amitesh Maiti of Molecular Simulations, Inc. for providing the $Mg_3(VO_4)_2$ (021) image shown in figure 1. Finally, we wish to thank Dr. Kenneth Poeppelmeier of Northwestern University for stimulating discussions regarding the reduction of magnesium orthovanadate materials.

Contents

Introduction

This report summarizes three years of research aimed at synthesizing and characterizing experimental models of magnesium orthovanadate oxidative dehydrogenation catalysts. The report is divided into three chapters, which either have been published or are in the process of being published in peer reviewed scientific journals. The first chapter (published in *Journal of Vacuum Science and Technology A*, vol. 18, July/August 2000, pp. 1928 – 1932) describes initial attempts to deposit thin, oriented films of magnesium orthovanadate. The second chapter describes the synthesis and characterization of these thin films in more detail, and discusses methods for controlling the oxygen content of the films. The final chapter describes experiments aimed at measuring and understanding the reactivity of the films toward molecules commonly used in oxidative dehydrogenation reactions. Each chapter contains a stand-alone introduction to the topic at hand, and the reader is referred to those sections for the rationale motivation for the work. Tables, figures, and references are given at the end of each chapter.

Chapter 1: Initial Deposition and Characterization of Oriented Magnesium Orthovanadate Thin Films

Introduction

Although magnesium vanadates are potentially important catalytic materials for the conversion of alkanes to alkenes *via* oxidative dehydrogenation [1, 2, 3], little is known about the active sites at which the catalytic reactions take place. Most studies to date have been conducted on powdered magnesium vanadate samples that consist of randomly oriented crystallites, and which may contain multiple crystalline phases and have irregular surface structures. The orientation, phase, and surface structure of the constituent crystallites all affect the surface reactivity, making it difficult to isolate the effect of any one feature on surface reactivity. In order to simplify the study of the magnesium vanadate surface reactivity, we require thin film samples that consist of a single magnesium vanadate phase and a well defined crystallographic orientation. Furthermore, it is desirable that the films be extremely thin (i.e., < 10 nm) and deposited on an electrically conducting substrate in order to eliminate charging effects during application of ultra high vacuum (UHV) surface analysis. A similar arrangement has even allowed for analysis of ultra-thin alumina films by scanning tunneling microscopy [4, 5]. Growth of such $Mg_3(VO4)_2$ films will reduce the complexity of the surface structure and greatly simplify the study of active sites in these important materials.

Magnesium orthovanadate, $Mg_3(VO4)_2$, was chosen as the target phase for synthesis due to a clear epitaxial relationship between the $Mg_3(VO_4)_2$ structure and the structure of several easily grown, well-oriented substrate materials. $Mg_3(VO_4)_2$ occurs in both a cubic [6]and an orthorhombic crystalline phase [7], but the orthorhombic phase is generally observed following preparation of $Mg_3(VO4)_2$ catalysts by calcining a 3:1 mixture of MgO and V_2O_5 in air [8]. Furthermore, this phase has been shown to be active in the oxidative dehydrogenation of propane [1,8]. Krishnamachari and Calvo have reported that the orthorhombic $Mg_3(VO_4)_2$ structure is based upon a pseudo-cubic structure of hexagonal close packed (hcp) layers of oxygen atoms [9]. The pseudo-hcp planes comprise the (042) set of crystalline planes which are separated by a d-spacing of 2.3559 Å. The average spacing between oxygen atoms within the pseudo-hcp net is 2.96 Å. Based on this structure, several materials were selected as potential seed layer materials on which to initiate epitaxial growth of $Mg_3(VO_4)_2$ oriented with the (042) plane parallel to the substrate. The candidate seed layer materials were selected for their hexagonal close packed geometry [either fcc (111) or hcp (0001)], strong preferential growth in that orientation, and minimal reactivity with $Mg_3(VO_4)_2$ at temperatures of up to 773 K. The resultant candidates are listed in Table I, along with their crystal structures, metal-metal spacing in the hcp planes, and relative lattice mismatch with the hcp (042) plane of oxygen in $Mg_3(VO_4)_2$. Although the seed layer materials generally exhibit strong preferential orientation with the hcp planes parallel to the plane of the substrate, their crystallites are probably randomly oriented within the plane of the substrate. In other words, the grains in the metal films are aligned with the hcp planes parallel to

the substrate but are rotated in plane with respect to one another. This strong preferential orientation in one direction only gives rise to a "fiber" texture in the films.

Experiment

Several $Mg_3(VO_4)_2$ thin films were deposited using RF reactive sputtering from stoichiometric ceramic targets. The films were deposited in a Unifilm PVD-300 Multisource Sputter System that allows sequential deposition from up to 5 sputter targets. This was especially useful in minimizing the lag time between deposition of a seed layer and the overlying $Mg_3(VO_4)_2$ film. By minimizing the lag time, we hoped to minimize contaminants on the pristine seed layer, thereby promoting epitaxial growth of the $Mg_3(VO_4)_2$ thin film deposited directly onto the crystalline seed layer. The base pressure of the system is ~ 2.0×10^{-7} Torr which results in deposition of a monolayer of residual gas contaminants on a pristine surface approximately every 5 seconds. All thin films were deposited using a chamber pressure of 10 mTorr. The source-to-substrate distance was 3.6 cm.

$Mg_3(VO_4)_2$ thin film samples were deposited onto oxidized Si wafers with and without seed layers to determine if preferential orientation could be forced. Si wafers were used as the substrates for Pt, Ag and Ti, while oxidized Si wafers were used as the substrates for Au because it reacted with the surfaces of non-oxidized Si wafers to form a silicide upon heating above 300°C. Seed layers, including Ti, Ag, Au, and Pt, were first deposited as single films onto oxidized Si wafers using the parameters listed in Table II. Standard θ-2θ x-ray diffraction (XRD) analysis was then performed to determine the crystalline orientation of the resultant seed layers. Seed layers that exhibited the preferred hexagonal close-packed orientation then were reproduced under identical conditions and coated immediately with an overlying thin film of $Mg_3(VO_4)_2$ without breaking vacuum.

$Mg_3(VO_4)_2$ thin films were deposited at temperatures of ~373 K (ambient) and 673 K in order to determine the effects of deposition temperature on the resultant crystalline structure. XRD was performed on these samples in order to assess crystallinity. In addition, the $Mg_3(VO_4)_2$ thin films were deposited in a reactive oxygen environment in order to ensure full oxidation of the thin films.

The bulk stoichiometry of the $Mg_3(VO_4)_2$ films was characterized using atomic absorption spectroscopy (AAS), while the surface stoichiometry was characterized using x-ray photoelectron spectroscopy (XPS). Samples were prepared for AAS by dissolving the $Mg_3(VO_4)_2$ film in concentrated HCl, and then diluting the resulting solutions prior to analysis on a Perkin Elmer 5100 PC instrument. XPS was performed using a VG Microtech Clam 2 operated at an analyzer resolution of 1.0 eV, with excitation provided by a VG Microtech XR3 Al Kα X-ray source. The XPS system is housed in a UHV chamber coupled to an atmospheric reactor, which allows treatment of the films in reactive environments typical of those found during oxidative dehydrogenation, followed by transfer to UHV without intervening exposure to air. Quantitation of the XPS results was performed using published sensitivity factors [10] and integrated areas under the Mg 2s, Mg 2p, and V 3p XPS peaks. These peaks were chosen rather than the more intense Mg 1s and V 2p peaks since these latter photoelectrons (particularly the Mg 1s peak) have relatively short inelastic mean free paths (IMFP), and are therefore subject to

severe attenuation by carbonaceous overlayers often formed during reaction in hydrocarbon containing mixtures. The Mg 2s, Mg 2p, and V 3p photoelectrons all have relatively long IMFPs and are therefore less susceptible to attenuation. Furthermore, these photoelectrons all have very similar kinetic energies, so that any attenuation that does occur is of similar magnitude for all of the peaks, and the relative areas of the peaks are unaffected.

The crystalline phase, orientation, and average crystallite diameter within the seed layers and the overlying $Mg_3(VO_4)_2$ films were determined using standard θ-2θ x-ray diffraction on a Siemens D-500 XRD. The usefulness of this technique is somewhat limited in this experiment because it only probes crystalline planes that are parallel to the substrate. In the case of a highly oriented sample, only one diffraction peak corresponding to a single d-spacing is detectable. This is especially problematic if both the seed layer and the overlying crystalline film are highly oriented and have equal d-spacings, as is the case for our samples. The XRD scans for $Mg_3(VO_4)_2$ films deposited onto highly oriented seed layers exhibit only one diffraction peak that could correspond to the seed layer, the overlying $Mg_3(VO_4)_2$ film, or both. In order to differentiate between signal generated from each of the two crystalline materials, we performed a more detailed XRD analysis on a Rigaku RTP-300 RC with an area detector collimated down to 100 μm. This XRD configuration enabled us to differentiate the signal generated from each of the thin film materials. Two samples were prepared for this analysis; a 50 nm Au seed layer film deposited at ambient temperature, and an identical Au seed layer with an overlying 200 nm $Mg_3(VO_4)_2$ thin film. By comparing the position and relative intensities of the resultant area XRD scans, we were able to verify the crystallinity of the overlying $Mg_3(VO_4)_2$ thin film.

Results and Discussion

Deposition of $Mg_3(VO_4)_2$ on Oxidized Si Wafers

$Mg_3(VO_4)_2$ thin films deposited to a thickness of 200 nm onto the amorphous surfaces of oxidized Si wafers are, in effect, amorphous themselves. The XRD scan from such a film deposited at 300 °C fails to exhibit any diffraction peaks corresponding to the thin film as shown in Figure 1. Only Si substrate diffraction peaks are visible on the scan. AAS and XPS analyses performed on this sample show a Mg/V atomic ratio of 1.50 ± 0.15, well within the uncertainty of the measurements, indicating that the films are stoichiometric as deposited.

Crystallinity of Seed Layers

50 nm Ti, Au, Ag and Pt thin film seed layers exhibit strong preferential orientation with the hexagonal close-packed lattice of atoms parallel to the substrates as expected. An XRD scan typical of the four thin film materials deposited onto oxidized Si wafers is shown in Figure 2. Deposition of Ti (300 °C) results in preferential growth in the (0001) (hcp) orientation, while deposition of Pt (300 ºC) and Ag (ambient) results in preferential growth along the (111) hcp orientation. Gold thin films deposited at 300 °C show several orientations including (200), (220), (111), and (311). However, deposition of a gold film at ambient temperature results in very strong preferential growth in the (111) hexagonal close-packed orientation as shown in Figure 2.

Deposition of $Mg_3(VO_4)_2$ on Seed Layers

200 nm $Mg_3(VO_4)_2$ thin films were deposited onto the four seed layer materials and analyzed using XPS and XRD in order to test for stoichiometry and crystalline structure and orientation. In addition, films of less than 10 nm thickness were also deposited on the titanium and gold seed layers for the reasons given in the Introduction. The seed layer on which the $Mg_3(VO_4)_2$ is deposited has a dramatic effect on the properties and behavior of the resultant $Mg_3(VO_4)_2$ thin film. $Mg_3(VO_4)_2$ thin films deposited onto Ag (111) seed layers at ambient temperature are extremely non-uniform in appearance. XRD scans of these samples show only the Si substrate peaks, suggesting that the $Mg_3(VO_4)_2$, Ag, and possibly the Si substrate have reacted to form an amorphous compound. Because of the amorphous nature of the films, deposition of $Mg_3(VO_4)_2$ onto Ag (111) was not pursued, and no further analysis was performed.

Deposition of $Mg_3(VO_4)_2$ thin films onto well-oriented (0001) Ti thin films results in a highly oriented crystalline structure with the (042) (pseudo-hexagonal) planes parallel to the substrate as indicated by XRD analysis, and the expected Mg/V ratio of 1.5 within experimental error as indicated by XPS analysis. However, deposition and subsequent heating of an 8.5 nm thick $Mg_3(VO_4)_2$ film on titanium to 300°C in 50 Torr of oxygen actually results in *reduction* of the V^{5+} to V^{3+} and complete destruction of the $Mg_3(VO_4)_2$ structure as evidenced by an increase in the Mg/V XPS ratio to ~3.0. We believe that these results indicate a reaction between the $Mg_3(VO_4)_2$ film and the titanium seed layer. Evidently, the affinity of titanium metal for oxygen is so high that it is able to extract oxygen from $Mg_3(VO_4)_2$ even under strongly oxidizing conditions, thereby effecting reduction of the vanadium and a disruption of the $Mg_3(VO_4)_2$ structure. Although we have achieved the goal of growing a highly oriented, single phase $Mg_3(VO_4)_2$ thin film on Ti (0001), titanium was rejected as a suitable substrate for the growth of ultra-thin, oriented $Mg_3(VO_4)_2$ films because of the reactivity between the two film materials.

In contrast to titanium, both gold and platinum have very low affinities for oxygen; neither metal forms an oxide upon heating in air. Thus, seed layers grown from these metals should not suffer from the reactivity problems observed for titanium. Deposition of $Mg_3(VO_4)_2$ onto well-oriented (111) Pt thin films resulted in a different orientation of the overlying $Mg_3(VO_4)_2$ crystallites. XRD analysis of this sample shows the $Mg_3(VO_4)_2$ (312) and possibly the (042) diffraction peaks as shown in Figure 3(a). That there are multiple for orientations for the overlying $Mg_3(VO_4)_2$ film is not surprising given the significant lattice mismatch (6.9%) between the ions in the $Mg_3(VO_4)_2$ (042) and Pt (111) hcp planes.

Deposition of a 200 nm $Mg_3(VO_4)_2$ layer onto Au (111) thin films results in $Mg_3(VO_4)_2$ thin films that exhibit the most preferential orientation in the desired configuration. Standard θ-2θ XRD was performed on these samples and the resultant scans show only two peaks; one corresponding to the Au (111)/ $Mg_3(VO_4)_2$ (042) planes and one corresponding to the Si (400) substrate as shown in Figure 3(b). This XRD scan is typical for $Mg_3(VO_4)_2$ thin deposited onto Au and Ti seed layers. Area XRD analysis also was performed on this sample in order to differentiate the signal resulting from the Au and $Mg_3(VO_4)_2$ thin films.

Area XRD scans were collected for an Au (111) seed layer film [Figure 4(a)] and an identically deposited Au (111) seed layer film with a $Mg_3(VO_4)_2$ film deposited on top [Figure 4(b)]. The signals were integrated over the same area (i.e. 2θ range) to enable direct comparisons of the relative intensities. On Figure 4(a), the very bright arc in the center of the area corresponds to the Au (111) planes that are oriented parallel to the substrate. The lower intensity arc to the left is the kβ radiation signal from the same set of planes. The very low intensity arc to the right corresponds to a small number of Au (200) planes that are oriented parallel to the substrate. The fact that nearly the entire signal is concentrated along the central Au (111) arc indicates that this Au thin film is very highly oriented with the (111) planes parallel to the substrate. The bright Laue spots correspond to the underlying, single crystal Si substrate. On Figure 4(b), the central arc has a much greater intensity than that of the Au seed layer only shown in Figure 4(a). The substantial increase in signal must result from a contribution from the overlying $Mg_3(VO_4)_2$ thin film. Given the nearly identical d-spacings between the $Mg_3(VO_4)_2$ (042) and the Au (111) sets of planes, $Mg_3(VO_4)_2$ epitaxially grown on the underlying Au seed layer would contribute to the signal in just this manner. The fact that no other diffraction arcs corresponding to $Mg_3(VO_4)_2$ crystallites appear indicates that the $Mg_3(VO_4)_2$ film is either epitaxial or completely amorphous. The increase in signal corresponding to a d-spacing of 2.35 Å indicates that the $Mg_3(VO_4)_2$ (042) planes are responsible for the additional signal. The relative intensities for the Au seed layer (4a) and the Au seed layer with an overlying $Mg_3(VO_4)_2$ film (4b) are plotted in Figure 4(c) for comparison.

XPS analysis of 1, 2, 4, and 200 nm thick $Mg_3(VO_4)_2$ films deposited onto the Au seed layers shows the desired surface stoichiometry in all cases. Furthermore, the films are thermally stable during treatment in vacuum, oxygen, or propane, provided reaction temperatures are kept below 500°C for the 4 and 200 nm films, and 400°C for the 1 and 2 nm films. Further details on the effects of reactive treatments will be given in chapters 2 and 3, but one result is of particular interest here. Wang *et al.* [11] showed that $Mg_3(VO_4)_2$ powders undergo a transformation to cubic spinel $Mg_3V_2O_6$ during high temperature reduction in hydrogen. This transformation occurs by a topochemical reaction which leaves the psuedo-hcp arrangement of the oxygen atoms unchanged but alters the locations of the Mg and V cations. We have reproduced this experiment on the 200 nm $Mg_3(VO_4)_2$ on Au (111) film by treating the film in 100 Torr propane for 1 h at 500 °C. XPS shows complete reduction of $V^{5+}$to V^{3+} and XRD of the reduced film shows (111), (222), and (444) peaks of $Mg_3V_2O_6$ (Figure 5) exactly as expected for topochemical conversion of an (042) oriented $Mg_3(VO_4)_2$ film into a (111) oriented $Mg_3V_2O_6$ film. This result not only supports the conclusion that the desired orientation of the $Mg_3(VO_4)_2$ film has been achieved, but also demonstrates that the films behave very much like bulk $Mg_3(VO_4)_2$ powders, and are therefore excellent model catalysts. The Au (200) and (220) diffraction peaks (Figure 5) are usually detectable using XRD following a thermal or reactive treatment of the samples. However, their intensity is always orders of magnitude lower than that of the Au (111)/$Mg_3(VO_4)_2$ (042) diffraction peak. Therefore, their presence does not indicate significant reconstruction of the Au seed layer film. Thus, it appears that the Au (111) seed layer is the most desirable from the standpoint of obtaining highly oriented, ultra-thin, stable films of $Mg_3(VO_4)_2$ with chemical properties similar to bulk $Mg_3(VO_4)_2$ powders.

Conclusions

We have successfully grown stoichiometric $Mg_3(VO_4)_2$ thin films oriented with the hexagonal (042) plane parallel to the substrate on a variety of conducting seed layers including Au (111), Ag (111), Pt (111), and Ti (0001). Based on the criteria of thermal stability and orientational order, Au (111) is the most desirable substrate material. Au does not react with $Mg_3(VO_4)_2$ and the films show excellent preferential (042) orientation. Furthermore, the films display chemical reduction behavior that closely resembles the behavior of bulk $Mg_3(VO_4)_2$ powders, indicating that these thin films are excellent models for bulk catalytic materials. We have determined that the ultrathin films do indeed minimize or eliminate charging effects typically encountered during electron and ion spectroscopy studies of oxides [11].

Table 1. Candidate "seed" layer materials for inducing epitaxial growth of $Mg_3(VO_4)_2$ (042).

Material	Crystal structure	hcp plane	Spacing in hcp plane (Å)	Lattice mismatch with $Mg_3(VO_4)_2$ (%)
Ti	hcp	(0002)	2.95	0.3
Ag	fcc	(111)	2.86	2.4
Au	fcc	(111)	2.88	2.8
Pt	fcc	(111)	2.77	6.9

Table 2. Deposition parameters for $Mg_3(VO_4)_2$ thin films and various metal seed layers.

Thin Film Material	Temperature (°C)	Ar flow (sccm)	O_2 flow (sccm)	Power (W)	Dep. Rate (nm/min)	Thickness (nm)
Ti	300	75	0	77 (DC)	5.9	50
Ag	Ambient	75	0	2.4 (DC)	7.7	50
Au	Ambient	75	0	4.3 (DC)	8.8	50
Au	300	75	0	4.3 (DC)	8.8	50
Pt	300	75	0	5.8 (DC)	7.2	50
$Mg_3(VO_4)_2$	300	75	2.5	241 (RF)	6.4	Varied

Figure 1. XRD scan of an $Mg_3(VO_4)_2$ film deposited onto an oxidized Si wafer. Only substrate diffraction peaks are visible, indicating that the overlying $Mg_3(VO_4)_2$ film is amorphous.

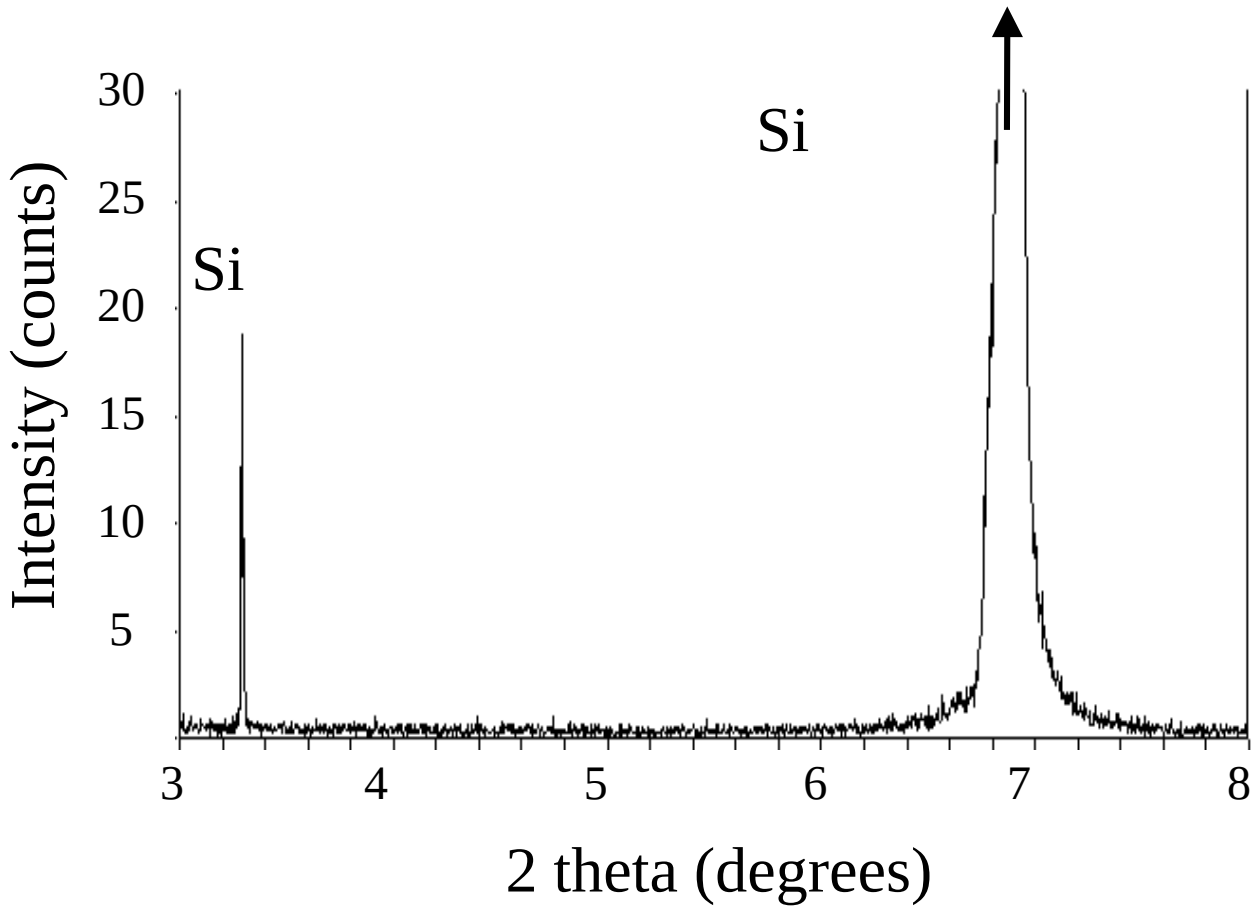

Figure 2 XRD scan of an Au film deposited at ambient temperature onto an oxidized Si wafer. Only the substrate and Au (111) diffraction peaks are visible, indicating a highly oriented Au thin film. Similar XRD scans are obtained for the other seed layer materials.

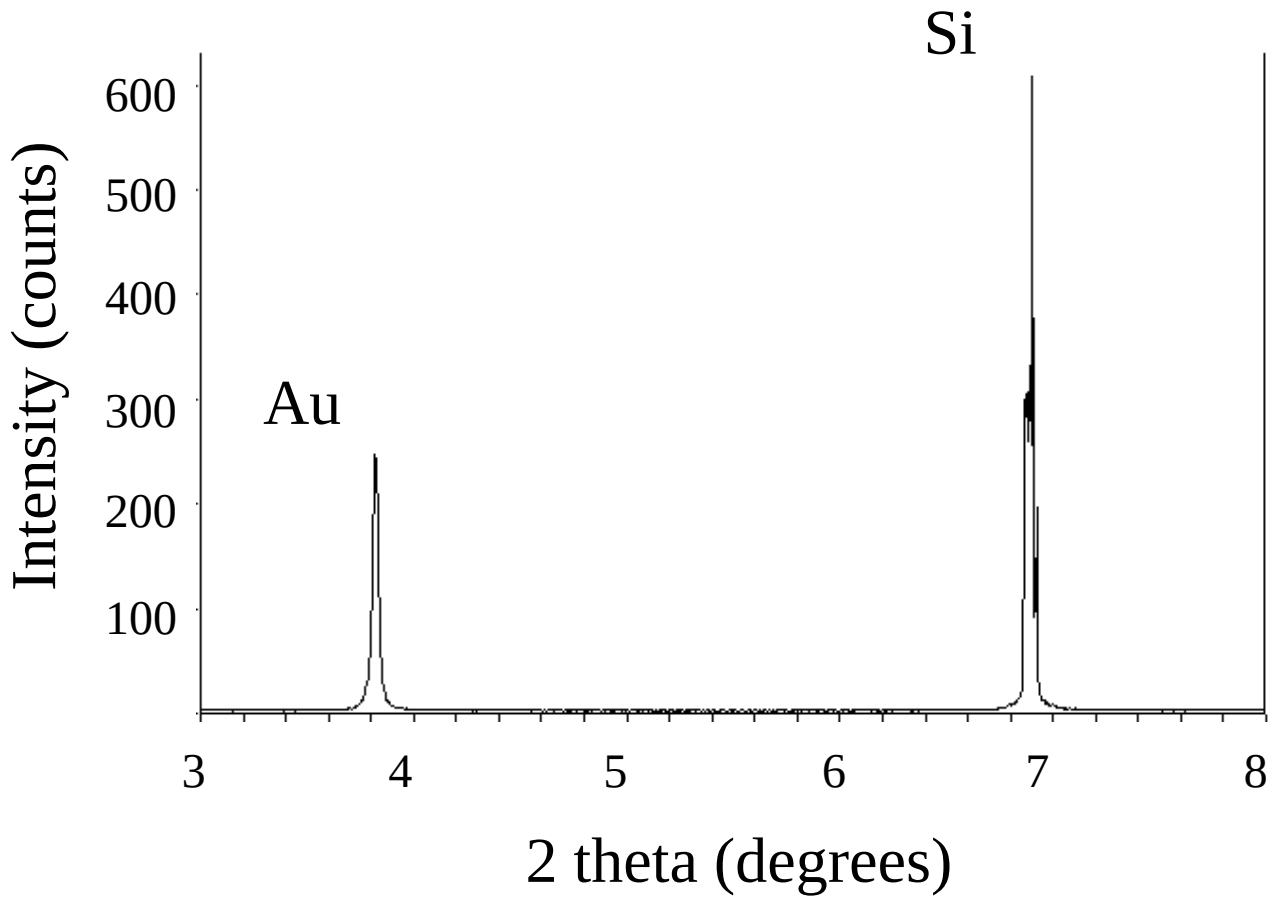

Figure 3(a) XRD scan of a 200 nm $Mg_3(VO_4)_2$ film deposited on a Pt seed layer at 300 ºC. Several $Mg_3(VO_4)_2$ peaks are visible indicating that $Mg_3(VO_4)_2$ is crystalline but randomly oriented.

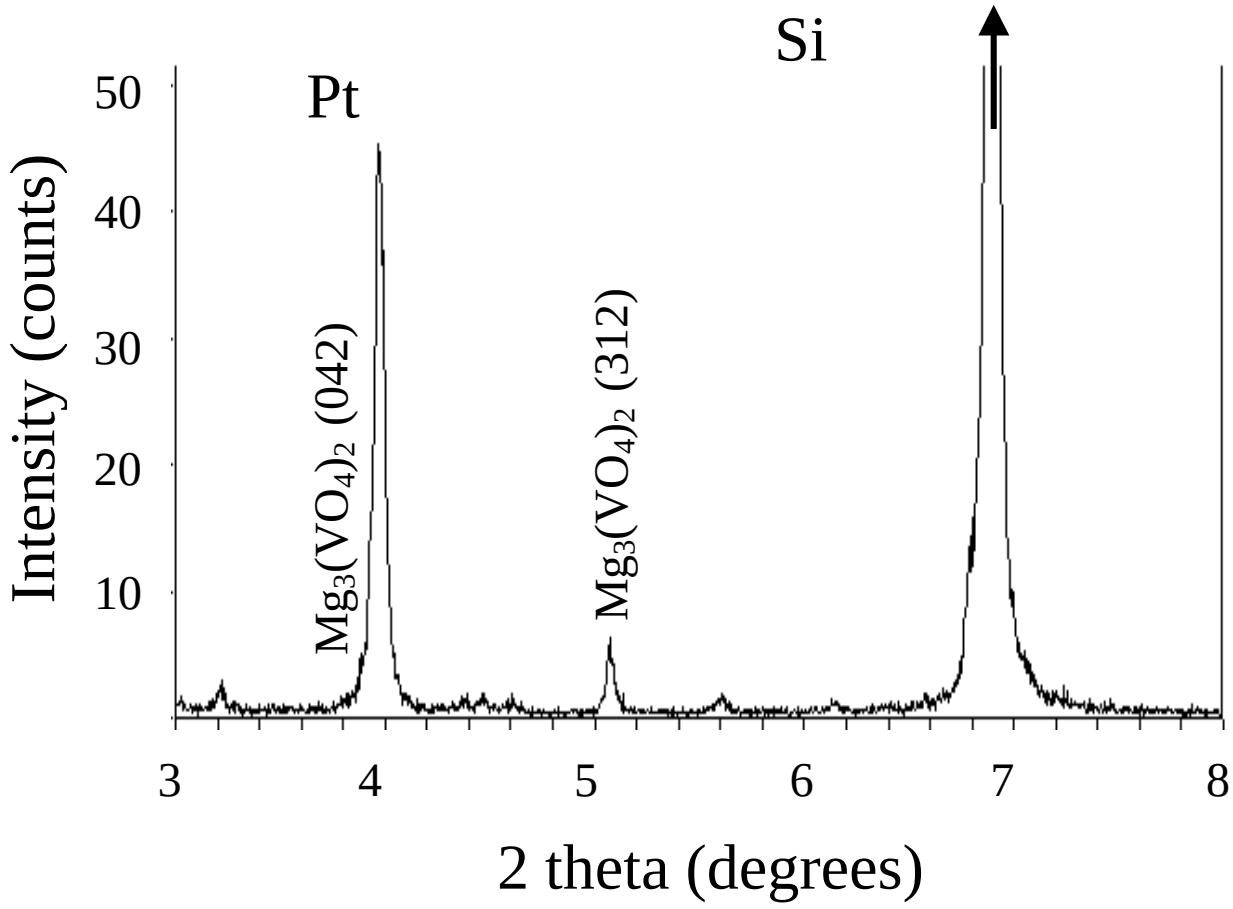

Figure 3(b) XRD scan of a 200 nm $Mg_3(VO_4)_2$ film deposited on an Au seed layer at 300 ºC. Only the substrate and Au (111)/ $Mg_3(VO_4)_2$ (042) diffraction peaks are visible, indicating that the Au and possibly the $Mg_3(VO_4)_2$ are highly oriented.

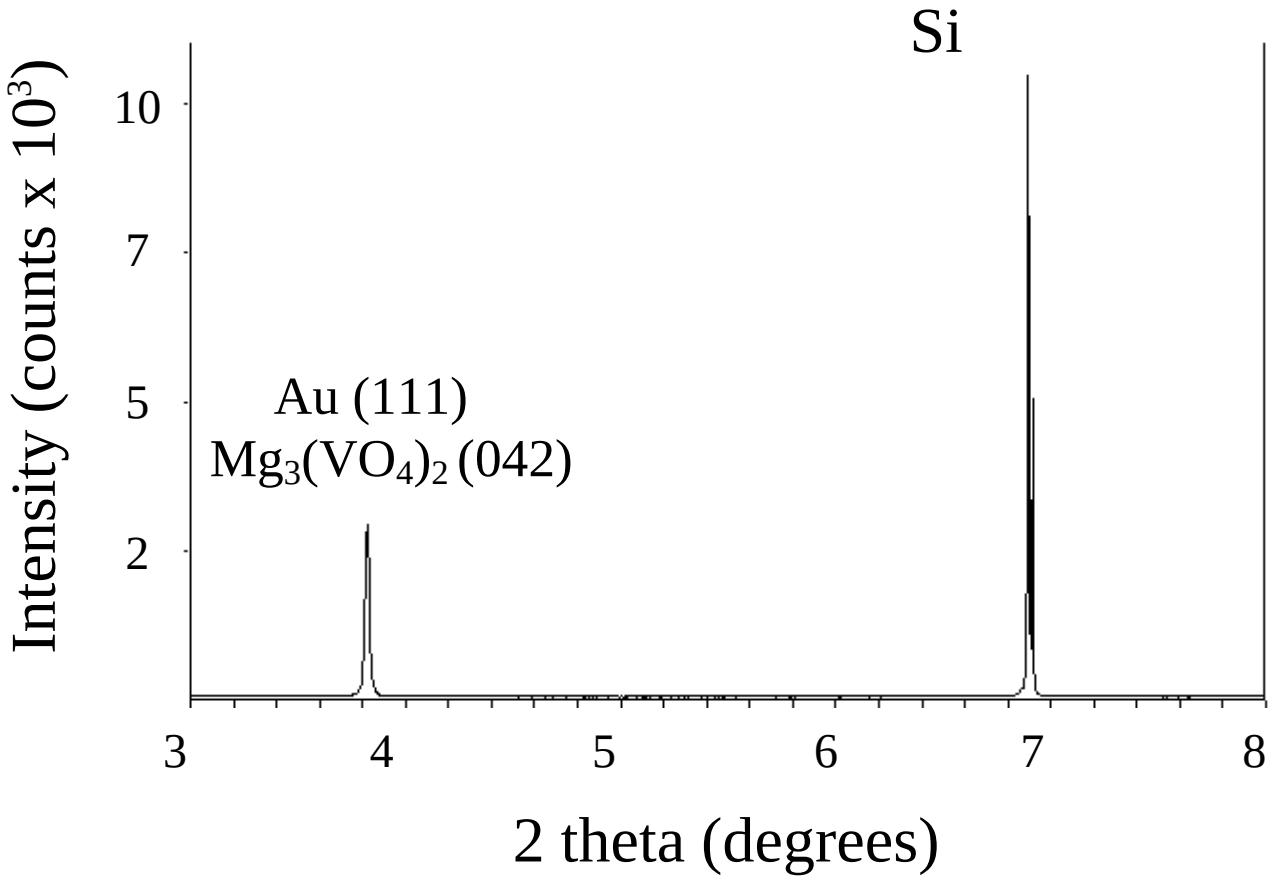

Figure 4(a) Area XRD scan of an Au seed layer deposited at ambient temperature. The bright arc in the center corresponds to the Au (111) set of planes parallel to the substrate.
Figure 4(b) Area XRD scan of an identically deposited Au seed layer with an overlying 200 nm $Mg_3(VO_4)_2$ thin film. The increase in signal of the central arc indicates that the $Mg_3(VO_4)_2$ is contributing to the intensity for the corresponding d-spacing (2.35 Å) and consequently must be preferentially oriented parallel to the substrate.

(a)

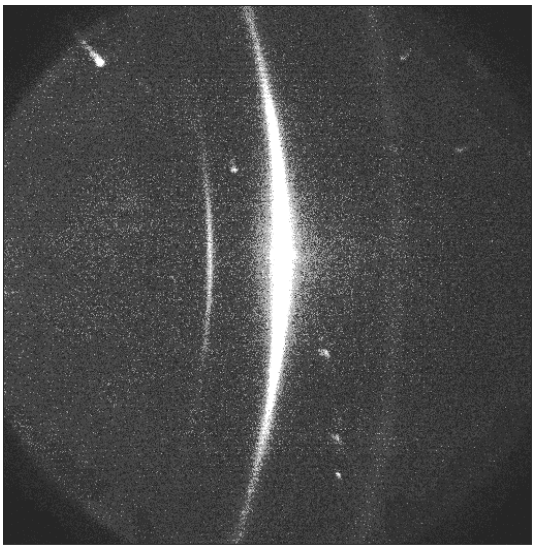

(b)

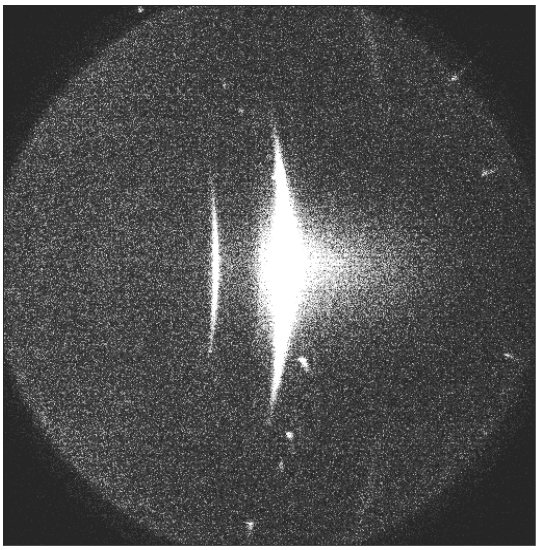

Figure 4(c) Integrated intensities of area XRD scans shown in (a) and (b).

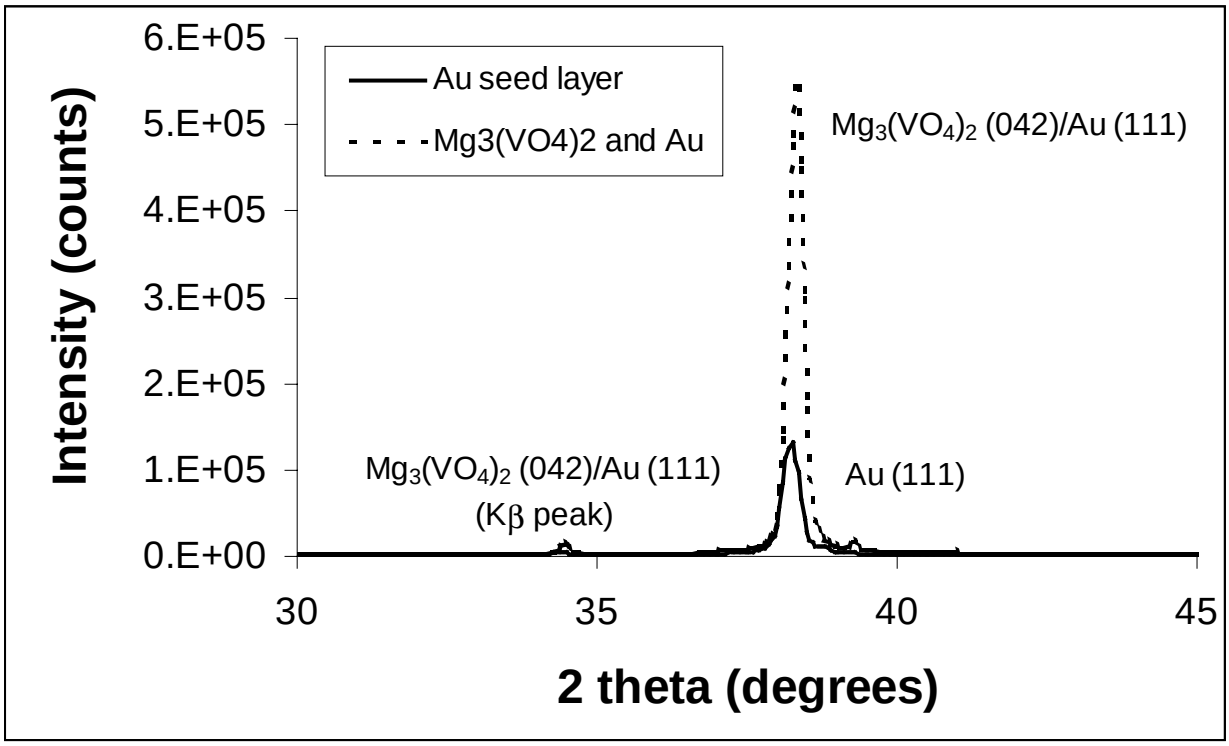

Figure 5 XRD scan of a film deposited as $Mg_3(VO_4)_2$ onto an Au seed layer and then reduced for 1h at 500°C in 100 Torr propane. The resultant scan shows several $Mg_3V_2O_6$ (reduced) diffraction peaks from the (111) planes.

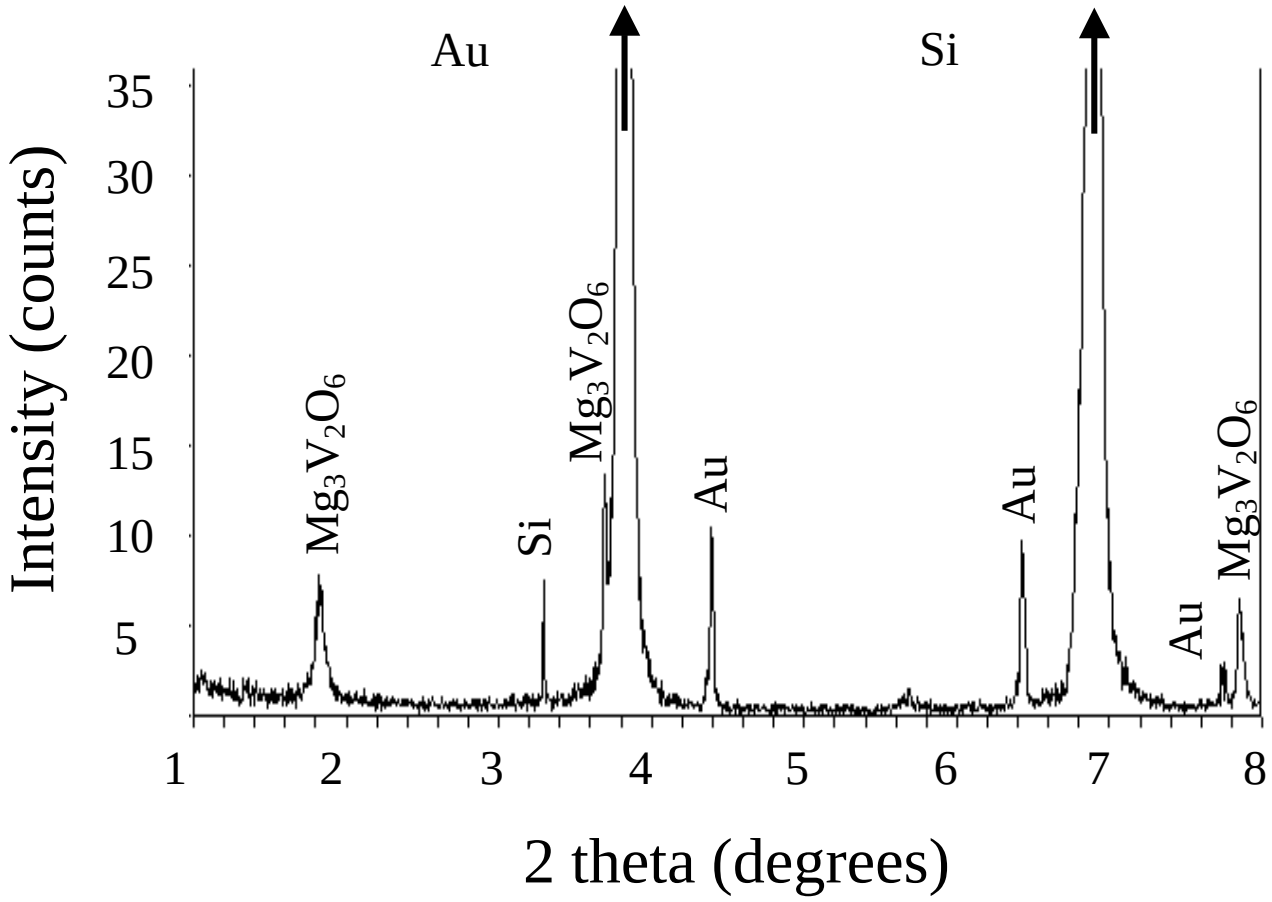

Chapter 1 References

1 H. H. Kung in "Advances in Catalysis," Vol. 40, (W. O. Haag, Ed.), Academic Press, Inc. (1991) p. 1.

2 M. A. Chaar, D. Patel and H. H. Kung, J. Catal. **109**, (1988) p. 463.

3 K. Seshan, H. M. Swann, R. H. H. Smits, J. G. van Ommen and J. R. H. Ross in "New Developments in Selective Oxidation" (G. Centi and F. Trifiro, Eds.) Elsevier Press, Amsterdam, (1990), p. 505.

4 J. Libuda, F. Winkelmann, M. Baumer, H.-J. Freund, Th. Bertrams, H. Neddermeyer, and K. Muller, Surface Sci. **318**, (1994) p. 61.

5 D. R. Rainer, C. Xu, and D. W. Goodman, J. Molec. Catal. **A119**, (1997) p. 307.

6 PDF card 19-0778, JCPDS – International Center for Diffraction Data, Newtown Square, PA.

7 PDF card 37-0351, JCPDS – International Center for Diffraction Data, Newtown Square, PA.

8 D. S. H. Sam, V. Soenen, and J. C. Volta, J. Catalysis **123**, (1990) p. 417.

9 N. Krishnamachari and C. Calvo, Can. J. Chem. **49**, (1971) p. 1629.

10 C. D. Wagner, L. E. Davis, M. V. Zoeller, J. A. Taylor, R. M. Raymond, and L. H. Gale, Surf. Interface Anal. **3,** (1981) p. 211.

11 X. Wang, H. Zhang, W. Sinkler, K. R. Poeppelmeier, and L. D. Marks, J. Alloys and Compounds **270**, (1998) p. 88.

Chapter 2: Controlled Variation of Oxygen Content of Oriented Magnesium Orthovanadate Thin Films

Introduction

Small alkenes such as ethene and propene are currently synthesized *via* steam cracking of natural gas liquids [1]. The large energy costs and low selectivities associated with this process motivates a search for more energy efficient processes. Potential alternatives include both oxidative and nonoxidative dehydrogenation. In nonoxidative dehydrogenation, thermal treatment of the alkane over a catalyst produces the alkene and hydrogen according to the reaction

$$C_nH_{2n+2} \rightarrow C_nH_{2n} + H_2 \qquad (1).$$

This endothermic reaction is equilibrium limited, necessitating high temperatures and low pressures to achieve adequate conversions. High temperatures not only require large energy input, but also decrease selectivity by promoting cracking reactions. In contrast, oxidative dehydrogenation (ODH) reacts the alkane with oxygen according to the reaction

$$C_nH_{2n+2} + O_2 \rightarrow C_nH_{2n} + H_2O \qquad (2).$$

Unlike nonoxidative dehydrogenation, ODH is exothermic and therefore not equilibrium limited, offering the possibility of low temperature operation and substantial energy savings. Of course, the thermodynamics of alkane/oxygen systems favors complete combustion to CO_2 and water so achievement of high selectivity is a major challenge for ODH.

Mixed-metal oxides are the most promising candidates for practical ODH catalysts. In all active mixed-metal oxide systems, multiple crystalline phases are known and synergistic effects between phases are generally observed. One commonly studied system, particularly for propane ODH, is magnesium vanadates. Three fully oxidized magnesium vanadate phases exist: $Mg_3(VO_4)_2$ (orthovanadate), $Mg_2V_2O_7$ (pyrovanadate), and MgV_2O_6 (metavanadate) [2,3,4]. In addition, a reduced $Mg_3V_2O_6$ phase has been reported [5], that was earlier observed but only identified as a cubic orthovanadate phase [6]. The preponderance of evidence suggests that the pyrovanadate is a superior propane ODH catalyst than the other two phases, but a recognized strong effect of catalyst preparation methods on performance makes it difficult to draw definitive conclusions regarding relative activity [2,3,4]. Furthermore, synergistic interactions between phases give rise to multiphase catalysts with performance superior to that of any of the individual phases [7]. Coupling the uncertainty regarding relative activity of the different phases with an almost complete lack of knowledge regarding which crystalline planes of the various phases are exposed in active catalysts renders identification of active sites extremely difficult.

Studies with well defined model catalysts would help to clarify this situation. In this paper we report on efforts to develop such model systems. Ideally, one would use single crystals of the mixed metal oxides, cut and polished to expose a single crystal plane, as model systems. This possibility is limited, however, both by the difficulty of growing high quality single crystals, as well as the insulating nature of the oxides which complicates the analysis of data from typical ultra-high vacuum (UHV) surface analytical probes. In the case of simple oxides, such as alumina, magnesia, and iron oxides, various workers [8,9,10] have utilized thin oxide films grown epitaxially on suitable substrates to overcome these problems. The films are thick enough to mimic the behavior of bulk materials, but thin enough so that they do not support static charging during surface analysis, to the point that scanning tunneling microscopy (STM) can be performed on the surfaces. Because suitable single crystals of mixed metal oxides are not available we are instead developing methods to epitaxially deposit oriented thin films of magnesium vanadates consisting of a single crystalline phase and exposing only a single crystal plane.

Our initial efforts in this area, reported in the previous chapter, involved the formation of thin films of magnesium orthovanadate exposing only the (021) plane. Although the magnesium orthovanadate structure is orthorhombic, consideration of the oxygen ions alone reveals a pseudo-cubic arrangement [11], with the magnesium and vanadium ions occupying select octahedral and tetrahedral sites, respectively. The (021) plane of $Mg_3(VO_4)_2$ is parallel to the close packed layers of oxygen ions, and therefore displays a distorted hexagonal symmetry, as shown in figure 1.

The symmetry of the $Mg_3(VO_4)_2$ (021) surface is well matched by the (111) surfaces of fcc metals, and good epitaxial growth of $Mg_3(VO_4)_2$ (021) surface could be expected on an fcc (111) metal surface with atomic spacing equal to the average O-O bond distance in the $Mg_3(VO_4)_2$ (021) surface. Among the several metals that meet this requirement, Au(111) provides an excellent substrate. In addition to a good epitaxial match, gold is also highly inert and does not react with the overlying $Mg_3(VO_4)_2$ (021) layer (see chapter 1). In the previous chapter we reported our initial efforts to sputter deposit epitaxial $Mg_3(VO_4)_2$ (021) films onto Au(111) surfaces, and demonstrated that both the desired Mg:V ratio and crystalline orientation were achieved. In this chapter we investigate the effects of oxygen flow rate during deposition on film quality. Specifically, we show that the films reported in chapter 1 were oxygen deficient and that films ranging from fully oxidized $Mg_3(VO_4)_2$ to heavily reduced $Mg_3V_2O_6$ can be produced depending upon deposition conditions. In the next chapter we will report on the chemical reactivity of our films under conditions encountered during ODH reactions.

Experimental

Full details of the film deposition process are provided in chapter 1, so only a brief overview of the procedures are given here. Au(111) substrates were obtained by DC sputter deposition of 50 nm gold films onto polished Si wafers covered by a 4000 Å thick thermally grown oxide layer. By employing oxidized Si wafers, we avoid reaction between Si and Au to form silicides, which disrupts the orientation of the Au films. Au films naturally align themselves to expose the desired (111) surface since the close-packed arrangement of oxygen atoms in this plane maximizes coordination number at the surface and minimizes surface free

energy. Note that the Au(111) substrate formed by this procedure is not a single crystal surface, but rather a polycrystalline surface in which the exposed (111) surfaces of each crystallite are rotationally disordered with respect to each other. Preliminary atomic force microscopy (AFM) measurements suggest that the crystallites are on the order of 30-40 nm in size.

200 nm thick $Mg_3(VO_4)_2$ films were deposited onto the Au substrates using reactive rf sputtering from a stoichiometric ceramic target. A nominal deposition rate of 6.4 nm/min. was employed and oxygen flow rate during deposition was varied from 0.0 sccm to 7.5 sccm. Our previous work provides further details of the deposition process, extensive X-ray diffraction (XRD) analysis demonstrating that the desired (021) film orientation is achieved by our deposition process, and chemical analysis showing achievement of the proper stoichiometry. Like the starting Au(111) substrates the oriented $Mg_3(VO_4)_2$ films are not single crystals, but rather polycrystalline surfaces with random rotational orientation of the individual exposed (021) planes.

Film structure and composition were analyzed by XRD, Fourier transform Infrared (FTIR) spectroscopy, and X-ray photoelectron spectroscopy (XPS). XRD was performed using standard θ-2θ x-ray diffraction on a Siemens D-500 XRD. A Nicolet 20SXB Fourier transform infrared spectrometer equipped with a SpectraTech COLLECTOR^{TM} diffuse reflectance accessory was used to obtain FTIR spectra of the films. Although this accessory is not designed for specular reflectance measurements, we have found that high quality reflectance spectra can be obtained provided the angle of incidence is adjusted so that the IR beam penetrates the film and is reflected off the underlying gold layer rather than off the surface of the $Mg_3(VO_4)_2$ films. Samples were mounted by placing a small piece of the coated Si wafer on top of the diffuse reflectance sample cup and adjusting the optics to maximize signal. Background spectra were obtained from an oxidized Si wafer coated with a 50 nm Au film, deposited in an identical fashion to those used as substrates for the $Mg_3(VO_4)_2$ films.

XPS was performed using a VG Microtech Clam 2 operated at an analyzer resolution of 1.0 eV, with excitation provided by a VG Microtech XR3 Al Kα X-ray source. Identification of V oxidation states by XPS is somewhat problematic, as pointed out by Gao *et al*. [4]. While the $2p_{3/2}$ binding energy of V^{5+} is generally agreed to be between 517.1 and 517.6 eV, the discrimination between V^{4+} and V^{3+} is not as clear. Gao *et al*. [4] assign a peak at 515.5 eV to V^{4+}, but in the present work we assign this peak to V^{3+} since it appears in samples that are known by XRD to contain V^{3+} in the form of $Mg_3V_2O_6$ (see below). Also, Burrows *et al*. [12] report V^{3+} formation, but no V^{4+}, upon reduction of $Mg_3(VO_4)_2$ in a rich propane/oxygen environment. Nevertheless, the possibility of some V^{4+} at the surface cannot be completely discounted. For fully oxidized films, binding energies were referenced to the V $2p_{3/2}$ peak at 517.6 eV, corresponding to V^{5+}. Fully oxidized films were identified by the presence of a sharp, symmetrical V $2p_{3/2}$ peak 13.0 ± 0.1 eV below the O 1s peak. Oxygen deficient films generally display a broad peak consisting of both V^{5+} and V^{3+}. The oxygen deficient films have a relatively high electrical conductivity, and do not exhibit any charging during XPS.

For comparison purposes, a powder sample of $Mg_3(VO_4)_2$ was prepared using the citrate method described by Delmon and coworkers [4,13]. A transparent solution of $Mg(NO_3)_2$ and NH_4VO_3 in the proper stoichiometric ratio was treated with citric acid in an amount to give a

10% molar excess of anions over cations. The solution was evaporated in a rotovap at 40°C to obtain a viscous material and then dried at 80-90°C to obtain a solid. The dry solid was decomposed at 380°C for 18 h and then calcined at 550°C for 6 h. The resulting powder possesses a surface area of 25.5 m^2/g and gives the powder XRD pattern expected for $Mg_3(VO_4)_2$ with no detectable impurities. An FTIR spectrum of the $Mg_3(VO_4)_2$ powder was obtained by mixing the powder with ground KBr to give 5 wt% orthovanadate, and then filling the sample cup of the FTIR diffuse reflectance accessory with the mixture. A background for the $Mg_3(VO_4)_2$ powder spectrum was obtained from pure KBr powder.

Results and Discussion

Figure 2 shows XRD of the oriented films as a function of oxygen flow rate during deposition. For films deposited with oxygen flow rates of 1.0 sccm or greater, XRD shows a peak at d ≈ 2.35 Å that is a combination of the Au (111) and $Mg_3(VO_4)_2$ (042) diffraction peaks, as demonstrated in the previous chapter. Peaks corresponding to Si (400) from the substrate are the only other features observed. For oxygen flow rates below 1.0 sccm an additional peak appears at d ≈ 2.10 Å. This peak corresponds to the (400) diffraction peak of the reduced $Mg_3V_2O_6$ phase [5], indicating that these films are highly oxygen deficient.

XPS experiments support the formation of $Mg_3V_2O_6$ at low oxygen flow rates (see figure 3). While the film prepared in the absence of oxygen initially displays a mixture of V^{5+} (517.6 eV) and V^{3+} (515.6 eV) near the surface, mild heating in vacuum to 673K for 5 minutes results in complete conversion of all near surface vanadium to V^{3+}. Films deposited with oxygen flow rates above 1.0 sccm show only V^{5+} initially, and little or no conversion to reduced V upon heating in vacuum. These results are entirely consistent with formation of $Mg_3V_2O_6$ in the film deposited in the absence of oxygen. Exposure of the film to air upon removal from the deposition chamber is expected to oxidize any reduced V formed in the near surface region during deposition, resulting in observation of V^{5+} by XPS even if the as-deposited film contains only V^{3+}. Mild heating in vacuum easily reverses the surface oxidation through oxygen desorption, converting V^{5+} in the near surface region back to V^{3+}. For fully oxidized films, mild heating in vacuum also likely results in oxygen desorption, but in this case the oxygen vacancies diffuse into the bulk and the corresponding reduced V species are found throughout the bulk of the film rather than at the surface.

The formation of oxygen vacancies during deposition is also reflected in the electrical conductivity of the films. Pantazidis *et al*. [14] have shown that reduction of $Mg_3(VO_4)_2$ results in order of magnitude increases in bulk electrical conductivity, and that the conductivity can be ascribed to anionic oxygen vacancies. We see similar changes in the conductivity of our films as the extent of oxidation decreases. Fully oxidized films exhibit moderate sample charging during XPS, resulting in binding energy shifts of ~2 eV indicative of relatively low conductivity. Highly oxygen deficient films exhibit no charging, indicating a substantial increase in conductivity. For the sample deposited with 2.5 sccm O_2 an intermediate behavior occurs; the film initially exhibits modest charging of 0.9 eV, but after heating in vacuum charging no longer occurs. Thus, oxygen vacancy concentration clearly increases as oxygen flow rate decreases.

FTIR measurements shed further light on the extent of oxidation of the films. Figure 4 shows FTIR reflectance spectra of the films along with a diffuse reflectance spectrum of the orthovanadate powder for comparison. These spectra show major changes in vibrational properties as oxygen content increases. In contrast to XRD, which shows no changes for oxygen flow rates above 1.0 sccm, FTIR shows continued changes until a flow rate of 5.0 sccm is reached, indicating that fully oxidized films are not formed below this flow rate. The next chapter, which deals with film reactivity, will show significant differences between films deposited with 5.0 and 7.5 sccm O_2, suggesting that full oxidation is not achieved even at 5.0 sccm. In chapter 1 an oxygen flow rate of 2.5 sccm was employed. It is now clear that this flow rate produces slightly oxygen deficient films, and that the results reported in that chapter are not necessarily indicative of fully oxidized $Mg_3(VO_4)_2$. Nevertheless, the extent of oxidation is clearly quite high at 2.5 sccm and the evidence presented for the formation of an (021) oriented film remains valid.

For fully oxidized films, only a single broad, featureless peak at 957 cm^{-1} is observed by FTIR (figure 4e and 4f). As oxygen flow rate decreases this peak splits into two peaks at 967 and 924 cm^{-1}. At a flow rate of 0.3 sccm the 924 cm^{-1} peak shifts to lower frequency and increases in intensity relative to the 957 cm^{-1} peak. Simultaneously, a third peak appears at 666 cm^{-1}. In the absence of any oxygen, the two high frequency peaks are almost completely attenuated and the 666 cm^{-1} peak shifts to 715 cm^{-1}. The loss of intensity between 900 and 1000 cm^{-1} is of particular interest since this region corresponds to vibrational modes of VO_4 tetrahedra [5,15,16], which are present in $Mg_3(VO_4)_2$ but not in $Mg_3V_2O_6$ [5]. Thus, we conclude that the film deposited in the absence of oxygen contains little or no $Mg_3(VO_4)_2$, and is mainly composed of $Mg_3V_2O_6$. Similarly, the presence of VO_4 vibrational modes in the film deposited with 0.3 sccm O_2 suggests a mixture of $Mg_3(VO_4)_2$ and $Mg_3V_2O_6$. The correlation of the low frequency vibrational peak at 660 – 720 cm^{-1} with the presence of the $Mg_3V_2O_6$ (400) XRD peak (cf. figure 2) suggests that the peak at 650-700 cm^{-1} arises from a vibrational mode of $Mg_3V_2O_6$. Similar results were obtained by Wang *et al.* [5].

Comparison of FTIR spectrum of the fully oxidized film with that of $Mg_3(VO_4)_2$ powder reveals major differences, attributable to the high degree of orientation of the fully oxidized films. Evidently the orientation of certain bonds relative to the surface, coupled with the geometry of our FTIR reflectance accessory, prevents excitation of vibrational modes in the region between 600 and 800 cm^{-1} and alters the relative intensity of the modes above 800 cm^{-1}. A similar, though less dramatic effect was reported by Finke and Schrader for poly(methylmethacrylate) films [17].

The growth of the reduced $Mg_3V_2O_6$ phase from a fully oxidized ceramic target requires some explanation since conservation of mass dictates that the overall composition of the sputtered particles must equal the bulk composition of the target [18]. According to Waits [19], oxides are broken up into their component atoms and suboxides during sputtering. Oxygen often has a lower sticking coefficient on the substrate than the metal atoms and consequently the resultant films are oxygen deficient. Supplying additional oxygen in the gas phase during deposition reverses this effect and allows the deposition of fully oxidized films.

It is remarkable that the $Mg_3V_2O_6$ phase deposited in the absence of oxygen grows in a (100) orientation given the close relation between the $Mg_3V_2O_6$ and $Mg_3(VO_4)_2$ structures. Conversion from the orthovanadate to the reduced phase occurs through migration of the metal ions to different sites, but with retention of the cubic oxygen ion lattice (see figure 4 in ref [5]). As a result the structure changes from orthorhombic to cubic and the (021) planes in the orthovanadate phase become (111) planes in the reduced $Mg_3V_2O_6$ phase. This transformation was reported in chapter 1 where it was shown that severe reduction of a (021) oriented $Mg_3(VO_4)_2$ film results in formation of a (111) oriented $Mg_3V_2O_6$ film. Thus, one might expect that direct growth of $Mg_3V_2O_6$ on Au(111) would result in a (111) orientation rather than the observed (100) orientation. The observed formation of the (100) surface is most likely due to an unanticipated epitaxial relationship between the Au(111) and the $Mg_3V_2O_6$ (100) surfaces. In figure 5 we show an overlay of a cubic (111) surface with a cubic (100) surface having the same lattice parameter. The match in the x direction is necessarily exact, but there is also an almost perfect coincidence between the two lattices in the y direction. After a distance of six lattice parameters in the y direction the vertices in the (111) and (100) surfaces line up with a mismatch of only 1.04%. The presence of this coincidence helps to explain the epitaxial formation of (100) rather than the (111) surfaces of $Mg_3V_2O_6$, although it is likely that other factors, including differences in surface free energy between the (100) and (111) surfaces, also play a role.

From the relationship between the structures of $Mg_3V_2O_6$ and $Mg_3(VO_4)_2$, one would expect oxidation of $Mg_3V_2O_6$ (100) to result in formation of an $Mg_3(VO_4)_2$ (001) surface. Attempts to oxidize the $Mg_3V_2O_6$ (100) film in 50 Torr O_2 at 773 K for several hours failed to convert the $Mg_3V_2O_6$ (100) film into the orthovanadate. While XPS measurements show full oxidation of the $Mg_3V_2O_6$ (100) surface, XRD measurements continue to show the $Mg_3V_2O_6$ (400) peak with no evidence for the $Mg_3(VO_4)_2$ (004) peak. FTIR spectra show noticeable changes upon oxidation, including increased intensity in the region from 800-1000 cm^{-1} consistent with the formation of tetrahedrally coordinated vanadium. Thus, it is possible that some $Mg_3(VO_4)_2$ formation occurred during oxidation, but either the extent was not great enough to be observed in XRD, or the conversion did not occur with retention of the orientation of the cubic oxygen lattice.

Conclusions

By controlling oxygen flow rates during sputter deposition of $Mg_3(VO_4)_2$ on Au(111), films ranging from fully oxidized $Mg_3(VO_4)_2$ to highly reduced $Mg_3V_2O_6$ can be formed. Both phases exhibit an epitaxial relationship with the underlying substrate, with orthorhombic $Mg_3(VO_4)_2$ adopting an (021) orientation, while cubic $Mg_3V_2O_6$ adopts the (100) orientation. FTIR appears to be a sensitive probe of film oxidation. Continuous changes in the FTIR spectrum as the oxygen flow rate increases demonstrate that $Mg_3(VO_4)_2$ formation persists to very low oxygen flow rates, and that oxygen flow rates in excess of those used previously are required to achieve full oxidation. In the next chapter, we will detail the reactivity of these films toward propane, oxygen, and propane/oxygen mixtures, demonstrate trends in reactivity with increasing oxygen deficiency, and relate the results to the catalytic properties of these materials for propane ODH.

Figure 1. Oxygen terminated (021) surface of $Mg_3(VO_4)_2$, showing hexagonal symmetry.

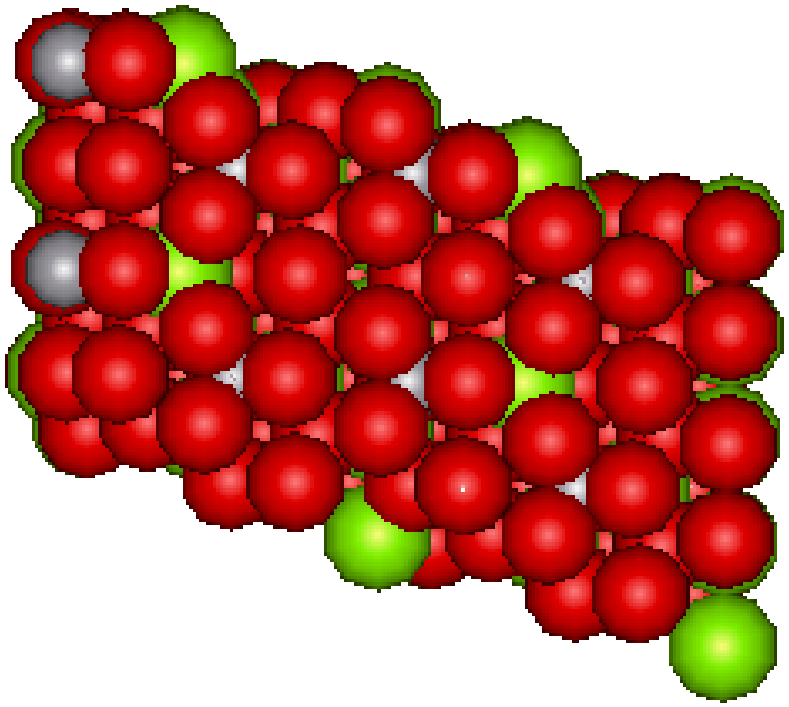

Figure 2. XRD of magnesium vanadate films as a function of oxygen flow rate: a) 0.0 sccm, b) 0.3 sccm, c) 1.0 sccm, d) 2.5 sccm, e) 5.0 sccm, f) 7.5 sccm.

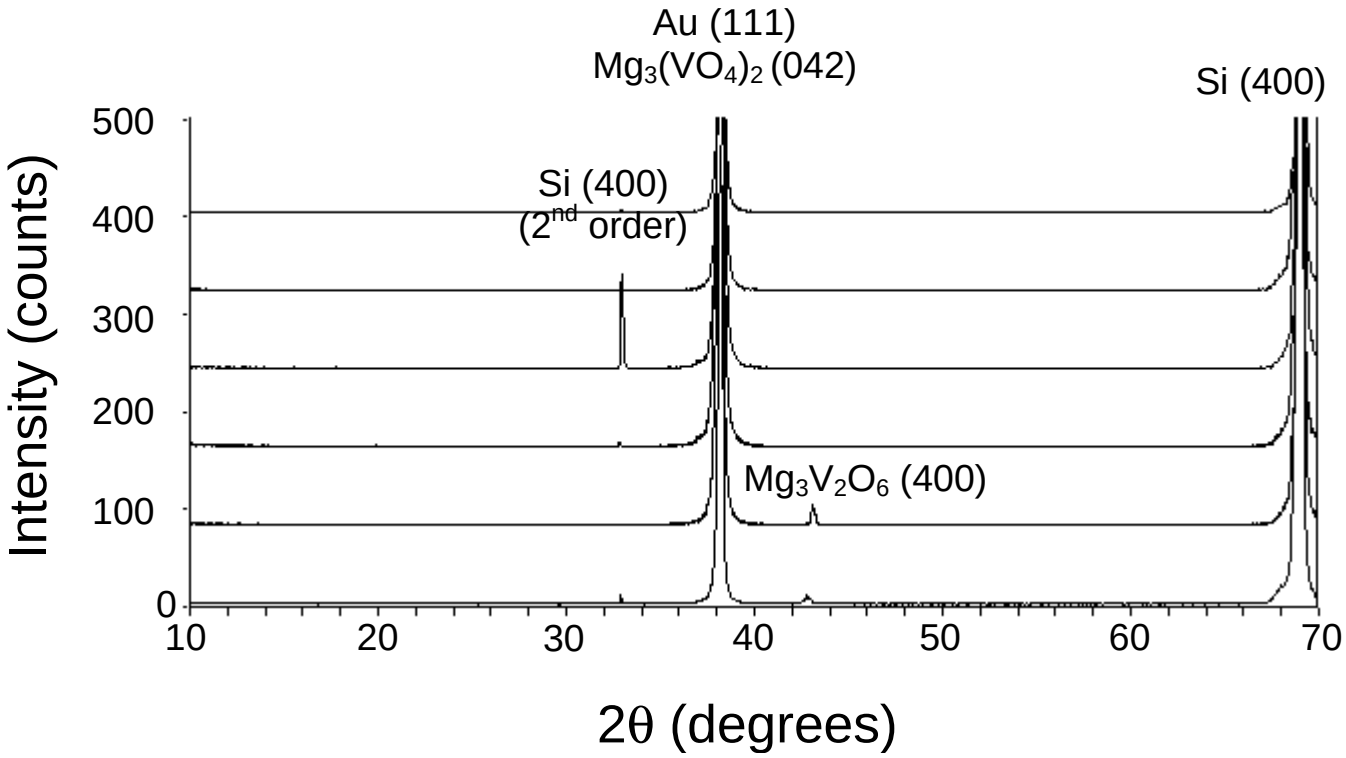

Figure 3. V 2p and O 1s XPS of magnesium vanadate films: a) film prepared with 0.0 sccm O_2, b) film prepared with 0.0 sccm O_2 after heating to 673K in vacuum for 5 min., c) film prepared with 5.0 sccm O_2, d) film prepared with 5.0 sccm O_2 after heating to 673K in vacuum for 5 min.

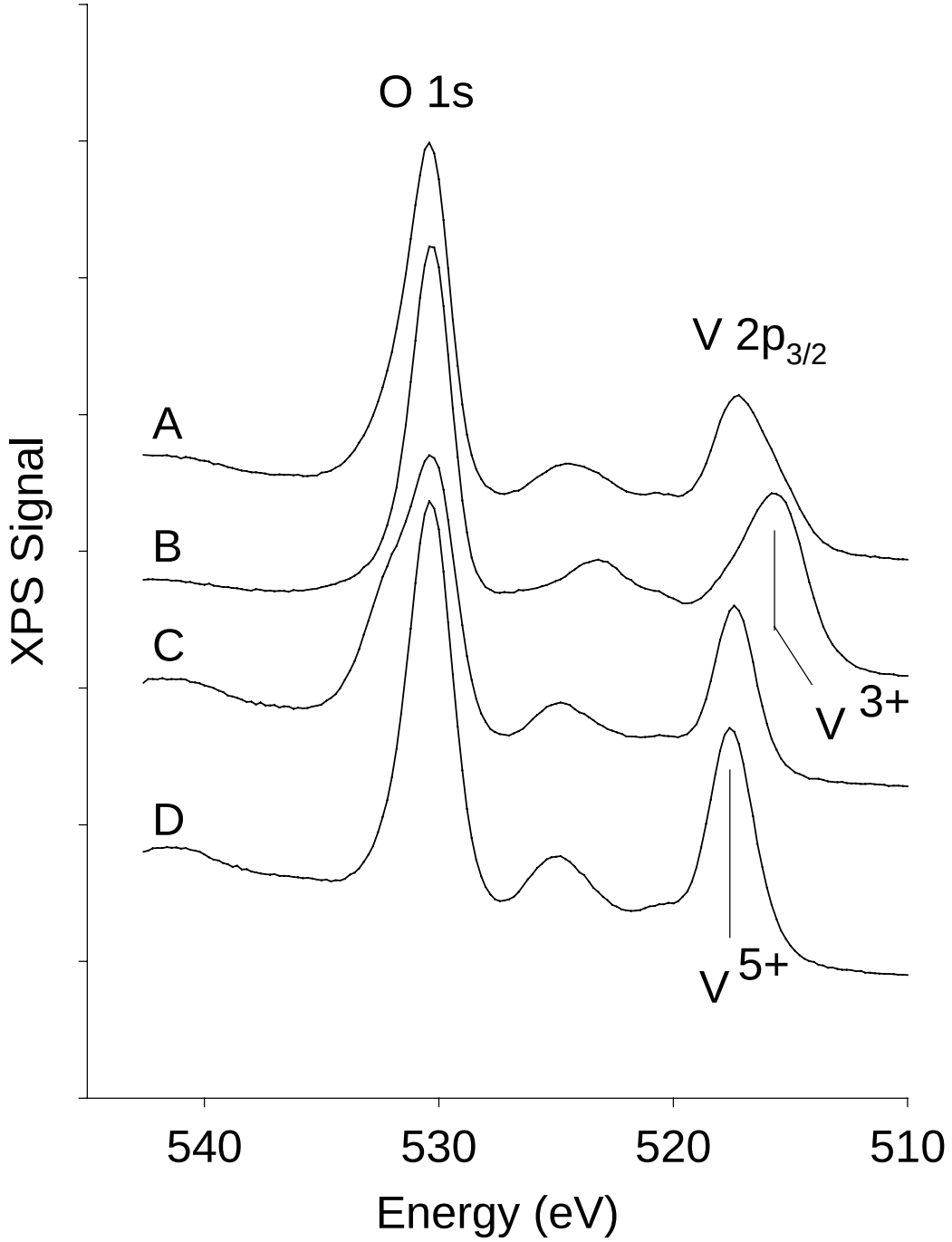

Figure 4. FTIR spectra of (021) oriented magnesium vanadate films as a function of oxygen flow rate: a) 0.0 sccm, b) 0.3 sccm, c) 1.0 sccm, d) 2.5 sccm, e) 5.0 sccm, f) 7.5 sccm, g) magnesium orthovanadate powder.

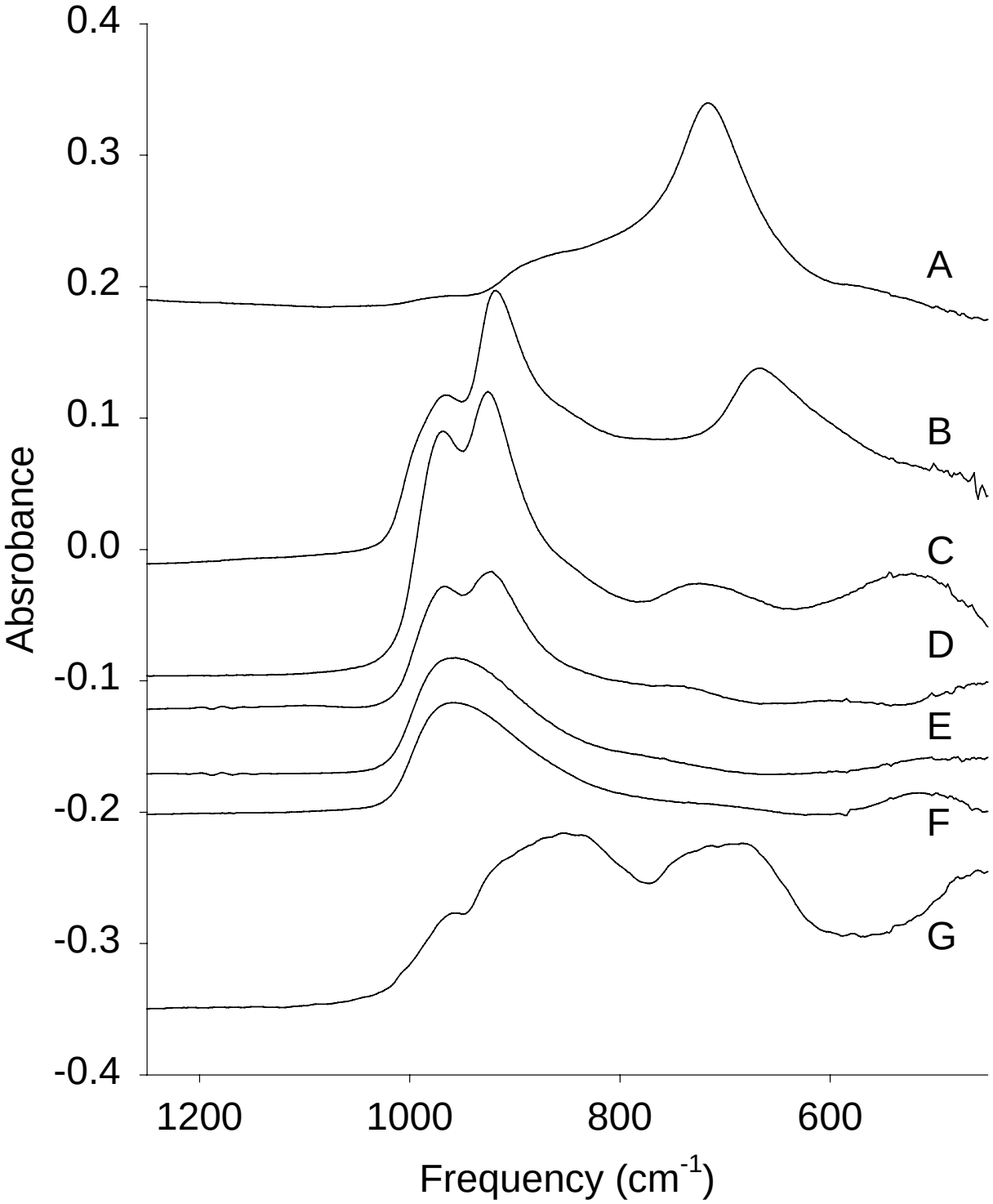

Figure 5. Schematic showing coincidence between (111) and (100) fcc surfaces with identical lattice parameters.

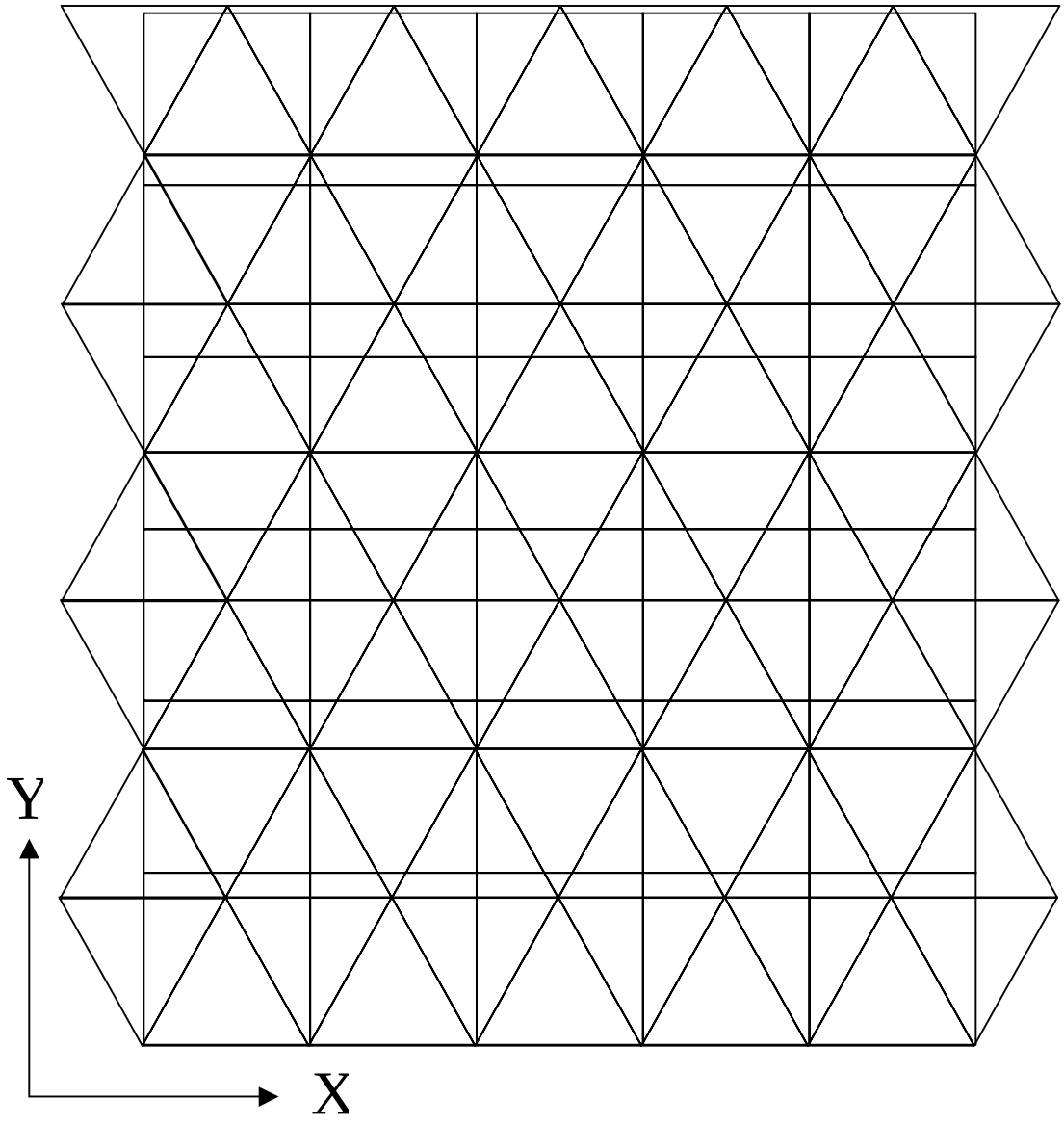

Chapter 2 References

1 J. G. Speight, “The Chemistry and Technology of Petroleum,” 2nd ed. (Marcel Dekker, Inc., New York, 1991) 726.

2 H. H. Kung, Adv. Catal., **40** (1994) 1.

3 D. Siew Hew Sam, V. Soenen, and J. C. Volta, J. Catal., **123** (1990) 417.

4 X. Gao, P. Ruiz, X. Guo, and B. Delmon, J. Catal., **148** (1994) 56.

5 X. Wang, H. Zhang, W. Sinkler, K. R. Poeppelmeier, and L. D. Marks, J. Alloys Cmpds., **270** (1998) 88.

6 PDF card 19-0778, JCPDS – International Center for Diffraction Data, Newtown Square, PA.

7 S. R. G. Carrazán, C. Peres, J. P. Bernard, M. Ruwet, P. Ruiz, and B. Delmon, J. Catal., **158** (1996) 452.

8 W. Weiss, M. Ritter, D. Zscherpel, M. Swoboda and R. Schlögl, J. Vac. Sci. Tech., **A16** (1998) 21.

9 F. Libuda, F. Winkelmann, M. Bäumer, H.-J. Freund, Th. Bertrams, H. Neddermeyer and K. Müller, Surface Sci., **318** (1994) 61.

10 X. Xu, S. Oh and D. W. Goodman, Langmuir, **12** (1996) 4877.

11 N. Krishnamachari and C. Calvo, Can. J. Chem. **49**, (1971) p. 1629.

12 A. Burrows, C. J. Kiely, J. Perregaard, P. E. Højlund-Nielsen, G. Vorbeck, J. J. Calvino, and C. López-Cartes, Catal. Lett., **57** (1999) 121.

13 Ph. Courty, H. Ajot, Ch. Marcilly, and B. Delmon, Powder Technol., **7** (1973) 21.

14 A. Pantazidis, A. Burrows, C. J. Kiely, and C. Miradatos, J. Catal., **177** (1998) 325.

15 E. J. Baran, Monatshefte für Chemie, **106** (1975) 1.

16 R. Iordanova, Y. Dimitriev, V. Dimitrov, and D. Klissurski, J. Non-Cryst. Solids, **167** (1994) 74.

17 S. J. Finke and G. L. Schrader, Spectrochimica Acta, **46A**, (1990) 91.

18 K. Wittmaack, in “Practical Surface Analysis,” 2nd Ed., Vol. 2, D. Briggs and M. P. Seah, eds. (John Wiley and Sons, New York, 1992) p. 124.

19 R. K. Waits, "Thin Film Deposition and Patterning", (American Vacuum Society, New York, 1998) p. 92.

Chapter 3: Reactivity of Oriented Magnesium Orthovanadate Thin Films

Introduction

Oxidative dehydrogenation (ODH) offers a potential energy saving route to formation of small alkenes such as ethene and propene. By reacting an alkane with oxygen under carefully controlled conditions, the exothermic ODH reaction offers the potential for higher conversions at lower temperatures than are possible with exothermic routes to small alkenes, such as steam cracking of natural gas liquids or non-oxidative dehydrogenation of alkanes. Because thermodynamics favor complete combustion of alkanes, selectivity becomes the major challenge in development of ODH catalysts.

ODH catalysts typically consist of complex mixed metal oxides systems that contain multiple crystalline phases, and possibly some amorphous surface phases as well. For example, magnesium vanadate catalysts, typically studied for propane ODH, can consist of as many as three different crystalline phases: $Mg_3(VO_4)_2$ (orthovanadate), $Mg_2V_2O_7$ (pyrovanadate), and MgV_2O_6 (metavanadate) [1,2,3]. Furthermore, synergistic interactions between phases may give rise to multiphase catalysts with performance superior to that of any of the individual phases [4]. Uncertainty regarding the distribution of the various phases, the relative exposed surface area of the individual phases, and the specific crystalline planes that are exposed, often frustrates attempts to obtain detailed atomic scale information regarding active site identity and properties.

In chapters 1 and 2 we reported the development of a model catalyst system that simplifies the complexity inherent in working mixed metal oxide catalysts. Our model system consists of a thin film of magnesium orthovanadate ($Mg_3(VO_4)_2$) epitaxially deposited such that only the (021) plane of the orthorhombic crystalline lattice is exposed. The desired epitaxy is achieved by rf sputter deposition of $Mg_3(VO_4)_2$ onto Au(111) surfaces. The (021) plane of the orthorhombic $Mg_3(VO_4)_2$ structure displays a pseudo-close packed geometry (figure 1, Chapter 2) with an average O-O spacing nearly equal to that of Au(111), resulting in an excellent epitaxial match. By eliminating the presence of multiple crystalline phases and exposing only a single crystalline plane, this model system offers the potential for performing a more detailed study of active site properties than previously possible.

Chapter 2 shows that the oxygen content of the magnesium vanadate films can be varied substantially by controlling oxygen flow rates in the sputtering chamber during deposition. Films varying from a reduced $Mg_3V_2O_6$ phase [5] to oxygen deficient $Mg_3(VO_4)_2$, to fully oxidized $Mg_3(VO_4)_2$ can be created. In this paper we report on the reactivity of these films toward oxygen, propane, and oxygen/propane mixtures at pressure and temperature conditions typically found in ODH reactors, and compare the behavior of the oriented films to that of amorphous films and bulk $Mg_3(VO_4)_2$ powders. The results demonstrate that the oriented films are excellent models of bulk $Mg_3(VO_4)_2$.

Experimental

Full details of the film deposition process are provided in chapter 1, so only a brief overview of the procedures are given here. As mentioned above, oriented films are prepared by deposition of $Mg_3(VO_4)_2$ onto Au(111) substrates. Polycrystalline Au(111) substrates were obtained by DC sputter deposition of 50 nm gold films onto polished Si wafers covered by a 4000 Å thick thermally grown oxide layer. $Mg_3(VO_4)_2$ films were deposited onto the Au substrates using reactive rf sputtering from a stoichiometric ceramic target. $Mg_3(VO_4)_2$ films thickness was nominally 200 nm. Oxygen flow rate during deposition was varied from 0.0 sccm to 7.5 sccm, with the extremes of the oxygen flow rate range corresponding to deposition of $Mg_3V_2O_6$ and fully oxidized $Mg_3(VO_4)_2$, respectively. The oriented $Mg_3(VO_4)_2$ films are not single crystals, but rather polycrystalline surfaces with random rotational orientation of the individual (021) planes.

In addition to deposition on Au(111), some films were also deposited directly onto oxidized Si wafers. Except for omission of the gold layer, deposition procedures for these films were identical to those for the (021) oriented films. X-ray diffraction (XRD) of all films deposited directly onto oxidized Si reveals the absence of any diffraction peaks other than those associated with the Si substrate. These films are therefore either amorphous or polycrystalline with randomly oriented crystallites so small that the XRD peaks are broadened to the point of being undetectable.

For clarity, we adopt the following nomenclature. Oriented samples will be designated MgVO-o(x.y), where the 'o' indicates an oriented film, and x.y indicates the oxygen flow rate (sccm) during deposition (*e.g.*, 0.0, 0.3, 1.0, etc.). Amorphous films will be designated MgVO-a(x.y), where the 'a' indicates an amorphous film and x.y indicates the oxygen flow rate. The use of the 'a' designation is solely designed to distinguish these films from the (021) oriented films, but the reader should bear in mind that we cannot preclude the possibility that the films are actually polycrystalline.

In addition to the thin film samples, a powder sample of $Mg_3(VO_4)_2$ was prepared using the citrate method [3,6]. This sample provides a standard against which the thin films samples will be compared to determine their suitability as models of bulk $Mg_3(VO_4)_2$ catalysts.

Film reactivity was analyzed by a combination of X-ray photoelectron spectroscopy (XPS), XRD, and Fourier transform Infrared (FTIR) spectroscopy. XPS was performed using a VG Microtech Clam 2 operated at an analyzer resolution of 1.0 eV, with excitation provided by a VG Microtech XR3 Al Kα X-ray source. The XPS system is housed in a UHV chamber coupled to an atmospheric reactor, which allows treatment of the films in reactive environments typical of those found during oxidative dehydrogenation, followed by transfer to UHV without intervening exposure to air. Samples were prepared by cleaving the Si wafers to form 13 x 7 mm pieces, which were then mounted by copper clamps on each side of the sample holder. Samples were heated by passing current directly through the samples. Temperature was measured using a Cr-Al thermocouple spot-welded to a small Ta clip that was press fit to the top edge of the sample.

Treatment in propane/oxygen mixtures involved isolation of the sample in the reactor, and sequential introduction of propane and oxygen to pressures of 100 and 50 Torr, respectively. The 2:1 propane:oxygen ratio is stoichiometric for the ODH reaction and the total pressure approximates that used in earlier studies of propane ODH in our laboratory [7]. The sample was heated to the desired temperature for the desired time in the reaction mixture and then cooled to room temperature while simultaneously evacuating the reactor. The sample was then transferred into the UHV chamber for XPS analysis. A similar procedure was employed for treatment in pure oxygen. Treatment in pure propane differed in that following the treatment the reactor was evacuated while holding the sample at the treatment temperature. With this procedure buildup of carbonaceous residue (which can interfere with XPS measurements) is minimized since weakly bound carbon containing species desorb during evacuation. Because heating in vacuum was found to be mildly reducing, this procedure was avoided during treatment in pure oxygen or oxygen/propane mixtures in order to minimize changes in the chemical state of the surface during evacuation.

Identification of V oxidation states by XPS has been discussed elsewhere in chapter 2 and elsewhere [3]. The $2p_{3/2}$ binding energy of V^{5+} is generally agreed to be between 517.1 and 517.6 eV, with the latter value being used in this work. We also observe a second V oxidation state with a binding energy of roughly 515.5 eV in reduced samples. In an earlier paper, we argue for assignment of this peak to V^{3+}, although others have assigned this peak to V^{4+} [3]. For the purposes of this paper, it is sufficient to state that this peak corresponds to a reduced form of V, without specifying the exact oxidation state. For fully oxidized films, binding energies were referenced to the V $2p_{3/2}$ peak at 517.6 eV, corresponding to V^{5+}. Fully oxidized films were identified by the presence of a sharp, symmetrical V $2p_{3/2}$ peak 13.0 ± 0.1 eV below the O 1s peak. Only fully or nearly fully oxidized films exhibit charging during XPS. Partially reduced or oxygen deficient films generally display a broad V $2p_{3/2}$ peak consisting of both V^{5+} and reduced V. These films have a relatively high electrical conductivity, and do not exhibit any charging during XPS.

Quantitation of the XPS results was performed using published sensitivity factors [8] and integrated areas under the Mg 2s, Mg 2p, and V 3p XPS peaks. These peaks were chosen rather than the more intense Mg 1s and V 2p peaks since these latter photoelectrons (particularly the Mg 1s peak) have relatively short inelastic mean free paths (IMFP), and are therefore subject to severe attenuation by adventitious carbonaceous overlayers invariably found on samples exposed to air or subjected to treatment in propane containing environments. The Mg 2s, Mg 2p, and V 3p photoelectrons all have relatively long IMFPs and are therefore less susceptible to attenuation. Furthermore, these photoelectrons all have very similar kinetic energies (~1380-1430 eV), so that any attenuation that does occur is of similar magnitude for all of the peaks, and the relative areas of the peaks are unaffected.

A Nicolet 20SXB Fourier transform infrared spectrometer equipped with a SpectraTech COLLECTOR™ diffuse reflectance accessory was used to obtain FTIR spectra of the films. Although this accessory is not designed for specular reflectance measurements, we have found that high quality reflectance spectra can be obtained provided the angle of incidence is adjusted so that the IR beam penetrates the film and is reflected off the underlying gold layer rather than off the surface of the $Mg_3(VO_4)_2$ films. Samples were mounted by placing a small piece of the coated Si wafer on top of the diffuse reflectance sample cup and adjusting the optics to maximize

signal. Background spectra were obtained from an oxidized Si wafer coated with a 50 nm Au film, deposited in an identical fashion to those used as substrates for the $Mg_3(VO_4)_2$ films. An attempt was made to obtain FTIR spectra of the amorphous films in a manner similar to that used for the oriented films. In this case background spectra were taken directly from a polished oxidized Si wafer. Unfortunately, the randomly oriented films displayed very weak absorption at the wavelengths of interest, and signal to noise ratios were not sufficient to allow meaningful data interpretation.

XRD was performed using standard θ-2θ x-ray diffraction on a Siemens D-500 XRD. Propane (Matheson, Research Grade, 99.97%) and oxygen (Matheson, Research Grade, 99.998%) were used as received without further purification.

Results and Discussion

Oriented Films

A major issue in using model systems to represent real catalysts is whether the chemical behavior of the simplified model system is sufficiently close to that of the real catalyst. In order to address this question we subjected the thin film model catalysts to treatments known to induce chemical and structural changes in the bulk orthovanadate. One treatment involves severe reduction of $Mg_3(VO_4)_2$. Wang *et al.* [5] showed that treatment of $Mg_3(VO_4)_2$ in hydrogen at 833K for 60h converts the orthorhombic orthovanadate into cubic $Mg_3V_2O_6$. Lubin and Rittershaus [9] also affected this conversion, reporting only the formation of a cubic orthovanadate phase. Finally, Burrows *et al.* [10] reported formation of this phase during reaction in a propane rich mixture at 773K, though they identify the phase as a cubic spinel, MgV_2O_4. Because Wang *et al*. performed a detailed structural analysis of the phase, we tend to favor their proposed stoichiometry over that of Burrows *et al*., but irregardless it is clear that a reduced cubic phase, containing only V^{3+} is formed upon treatment of $Mg_3(VO_4)_2$ under reducing conditions.

Accordingly, we subjected a 200 nm MgVO-o(2.5) film to 100 Torr propane at 773K for 2h. As shown in chapter 2, this film is initially somewhat oxygen deficient. As shown below, this oxygen deficiency enhances the reactivity of the film over that of fully oxidized films, and likely eases the transition to the reduced cubic phase. Figure 1 demonstrates quantitative reduction of V^{5+} in the near surface region of the film following this treatment. No evidence for V^{5+} remains by XPS after the propane treatment. Figure 2 shows qualitative agreement between the FTIR spectra of the reduced film and that of a film deposited in the absence of oxygen and shown in chapter 2 to contain the reduced $Mg_3V_2O_6$ phase. These two pieces of evidence, coupled with XRD data reported in chapter 1 showing the appearance of diffraction peaks from $Mg_3V_2O_6$, argues strongly for complete conversion of the $Mg_3(VO_4)_2$ film to $Mg_3V_2O_6$. Subsequent treatment of the reduced film in 50 Torr O_2 at 773K reverses the transformation, resulting in disappearance of the XRD peaks due to $Mg_3V_2O_6$ (see chapter 1), conversion of V^{3+} to V^{5+} (figure 1), and restoration of the original FTIR spectrum of the oriented $Mg_3(VO_4)_2$ film (figure 2). Burrows *et al*. [10] also report that the conversion is reversible, though this conversion becomes more difficult with the extent of ordering of the cubic phase. Altogether, it appears that the reduction behavior of the oriented $Mg_3(VO_4)_2$ film closely approximates that of

bulk $Mg_3(VO_4)_2$ powders, providing further evidence that the $Mg_3(VO_4)_2$ films are good model catalysts.

We next investigated the behavior of the oriented $Mg_3(VO_4)_2$ films under less severe reaction conditions. Specifically, we looked at the response of the films to treatment under stoichiometric reaction mixtures (2:1 mixture of propane and oxygen) at 673 and 773K, and in both pure oxygen and pure propane at 673K. Figure 3 shows the V 2p XPS of the MgVO-o(2.5) film as a function of cyclic reduction/oxidation treatments at 673K. At this temperature only partial reduction of vanadium occurs during treatment in propane, resulting in a shoulder at 515.5 eV on the low binding energy side of the V $2p_{3/2}$ peak. Subsequent oxidation reverses the reduction restoring the reduced V to the +5 oxidation state. Repeated cycling reproducibly results in partial conversion to reduced V during reduction, followed by reoxidation to V^{5+} during oxygen treatments. This reversible redox behavior is entirely consistent with the well-known Mars-Van Krevelen mechanism for oxidative dehydrogenation, whereby oxygen from the crystalline lattice of the catalyst is extracted by propane to form oxidation products, followed by replenishment of the oxygen vacancy, either by direct adsorption of oxygen from the gas phase at the vacancy site, or by adsorption of gas phase oxygen at a different site followed by diffusion of oxygen ions through the catalyst to the oxygen vacancy.

In figure 4, the effect of various treatments on the surface composition of the MgVO-o(5.0) film is shown. The initial surface composition of the film is identical to the bulk stoichiometry of $Mg_3(VO_4)_2$ within the measurement error of ±5%. A casual inspection of the figure clearly reveals two facts regarding the effects of reactive environments. First, surface composition can change substantially as a result of exposure to reactive environments. V/Mg surface ratios as low as 0.47 and as high as 0.78 were observed for this sample. More extreme values have been observed for other samples (see below). These deviations from the bulk stoichiometric ratio show that the surface compositions of $Mg_3(VO_4)_2$ ODH catalysts are not constant during reaction, and may in fact differ substantially from the bulk composition. Second, the sample response to a given treatment is highly dependent on previous history. For example, exposure to oxygen at 673K results in little or no change in surface composition when applied to a fresh sample, but results in a large decrease in V surface content when applied to a sample previously treated in propane/oxygen mixtures at 673 and 773K.

Not apparent in figure 4 is a direct correlation between changes in surface composition and V oxidation state. Increases in the V/Mg surface ratio are invariably accompanied by reduction of V with the extent of reduction roughly correlating with the percentage increase in the V/Mg ratio, and decreases in V/Mg ratios are invariably accompanied by oxidation of V. Applying this correlation leads to the conclusion that stoichiometric propane/oxygen mixtures change from oxidizing to reducing as the temperature increases from 673K to 773K. This result can be understood by considering that the reaction of propane with lattice oxygen to produce oxygen vacancies and reduced V, and the reoxidation of V, are two independent reactions with different activation energies. Reoxidation of vacancies has a lower apparent activation energy than the reaction of propane with lattice oxygen, such that at low temperatures reoxidation is faster, but at high temperatures reaction with propane is faster.

The preferential segregation of vanadium to the surface under reducing conditions is analogous to the observed spreading of reducible oxides on supported metal particles that occurs

as a result of strong metal-support interactions (SMSI) [11]. The SMSI phenomenon arises from the apparent ability of reduced forms of oxides, such as titania, to wet metal surfaces. Under strong reducing conditions titania is partially reduced and spreads over the surface of titania-supported metal particles. Upon reoxidation the titania can no longer wet the surface of the metal particles, resulting in either agglomerization of the titania into small, non-wetting patches on the metal surfaces, or diffusion of the titania off the metal particle surface and back into the support. A similar explanation is consistent with the increases in V/Mg ratios observed after reduction of the $Mg_3(VO_4)_2$ films. V^{5+} is partially reduced and becomes capable of wetting the $Mg_3(VO_4)_2$ surface. Upon reoxidation, V is converted back into V^{5+}, which either agglomerates into patches of V_2O_5 on the surface or diffuses back into the bulk of the $Mg_3(VO_4)_2$ film.

Figures 5 and 6 demonstrate the changes in surface composition resulting from reduction/oxidation cycles for films deposited with a range of oxygen flow rates. Figure 5 gives results when the initial treatment is reduction while figure 6 gives results when the initial treatment is oxidation. In both figures it is apparent that V reduction increases as oxygen flow rate during deposition decreases, at least for oxygen flow rates greater than 1.0 sccm. Also apparent is that films subjected to an initial reduction treatment display far greater variations in surface composition than those subjected to an initial oxidation treatment. For example, for sample MgVO-o(5.0) the initial reduction/oxidation cycle has little effect on surface composition but subsequent cycles shown increasing oscillations in the V/Mg ratio (figure 5). When the initial treatment is oxidizing (figure 6), this sample never displays any significant variation in the V/Mg ratio, even after the third oxidation treatment.

The history dependent behavior of the samples, as well as the increase in reducibility of the surface with decreasing oxygen flow rate during deposition, can be understood from consideration of the behavior of oxygen vacancies in $Mg_3(VO_4)_2$. Oxygen vacancies are clearly mobile in these materials, as evidenced by electrical conductivity measurements [12]. This oxygen vacancy mobility is widely believed to be key to the catalytic activity of mixed metal oxides, since it allow vacancies formed by reaction with alkanes to diffuse into the bulk and thereby eliminate oxygen vacancies at the surface. This behavior is likely responsible for the observation that ODH reactions occur on mixed metal oxides even in the absence of gas phase oxygen, with reaction rates declining only slightly even after an amount of oxygen equivalent to 50% of a monolayer has been consumed [1].

With this understanding, we can postulate that the increasing reducibility of the films with decreasing oxygen flow rate is related to the presence of oxygen vacancies formed during film deposition. Films deposited with high oxygen flow rates contain few oxygen vacancies. Upon reduction, oxygen vacancies are created at the surface but rapidly diffuse into the bulk, leaving the surface essentially fully oxidized. Films deposited with low oxygen flow rates contain relatively high concentrations of oxygen vacancies, but exposure to air following deposition fills oxygen vacancies located near the surface and results in a fully oxidized surface. Upon reduction oxygen vacancies are created at the surface, but because of the high vacancy concentration in the bulk there is no concentration gradient to drive diffusion of vacancies away from the surface. Instead, the vacancies remain at the surface resulting in detection of reduced V by XPS and spreading of a reduced V phase on the film surface.

The history dependent behavior of the samples is also explicable in terms of initial oxygen vacancy concentration. For all samples initial oxidation results in at least partial filling of oxygen vacancies formed during film deposition, thereby increasing the ability of the film to accommodate surface oxygen vacancies by diffusion into the bulk and decreasing the amount of reduced V observed following a subsequent reduction. Conversely, initial reduction results in increased concentrations of oxygen vacancies and segregation of reduced V to the surface. These changes are not completely reversed during a subsequent oxidizing treatment.

These effects must be purely kinetic in nature and not related to any equilibrium considerations. In an attempt to demonstrate the kinetic limitations, selected samples were subjected to reduction and oxidation cycles with treatment times doubled over those used to obtain figures 5 and 6. No significant changes in surface composition were observed as a result of the extended treatment times. This result can be explained by assuming that oxygen deficient films are in a thermodynamically unstable or metastable state following deposition. Depending upon the initial treatment, the films are converted into one of two more stable states, corresponding to a fully oxidized $Mg_3(VO_4)_2$ film (favored by initial oxidation), or an oxygen deficient $Mg_3(VO_4)_2$ film with reduced V species segregated to the surface (favored by initial reduction). Within this hypothesis, there must be a large kinetic barrier to conversion between the states. The MgVO-o(5.0) film provides an excellent example of bifurcation between the two states. This film is shown in chapter 2 to be only slightly oxygen deficient. Initial oxidation fills most of the oxygen vacancies and drives the film toward the fully oxidized state, which displays no significant response to subsequent reduction/oxidation treatments (figure 6). Initial reduction results in minor segregation of reduced V to the surface, but the extent of segregation increases with continued oxidation/reduction cycles as the sample is driven into the oxygen deficient state (figure 5).

It is important to note that the observation of reduced vanadium following reduction is not necessarily an indicator of reactivity toward propane. Experiments with bulk orthovanadate powder indicate that reaction rates are highest with fully oxidized orthovanadate [1]. The failure to observe reduced vanadium following reduction of fully oxidized films is the result of rapid replenishment of surface oxygen by diffusion of vacancies into the bulk, and not the result of slow reaction.

The above discussion is only valid when the film structure is that of $Mg_3(VO_4)_2$ containing a limited concentration of oxygen vacancies. When the oxygen flow rate during deposition falls below a critical value formation of the reduced $Mg_3V_2O_6$ phase begins, and the film can no longer be considered to have the defective $Mg_3(VO_4)_2$ structure assumed above. In this case the oxygen deficiency of the film is accommodated not by formation of oxygen vacancies in $Mg_3(VO_4)_2$, but by formation of $Mg_3V_2O_6$, which likely exhibits completely different reduction/oxidation behavior than the orthovanadate. This consideration explains the apparent anomalous behavior of the MgVO-o(1.0) sample seen in figures 5 and 6. While $Mg_3V_2O_6$ formation does not become apparent by XRD until oxygen flow rates fall below 1.0 sccm, it is likely that some $Mg_3V_2O_6$ is formed even at 1.0 sccm, though not to an extent detectable by XRD.

Included in figures 5 and 6 are results for the $Mg_3(VO_4)_2$ powder. The behavior of the MgVO-o(7.5) film is identical to that of the powder, suggesting that this film is fully oxidized

and therefore an excellent model for bulk $Mg_3(VO_4)_2$. The behavior of the MgVO-o(5.0) film diverges from that of the powder when subjected to an initial reduction treatment, indicating that this film is not fully oxidized.

Amorphous Films

Figures 7 and 8 compare the behavior of the oriented films with that of the amorphous films. For the fully oxidized films there is no significant difference between the oriented and amorphous films. As the oxygen deficiency of the films increases, the amorphous films display much smaller extents of reduction and V segregation than the oriented films. In fact, for the amorphous films decreasing the oxygen flow rate from 7.5 to 2.5 sccm appears to have no effect on the response of the films to oxidation and reduction treatments.

This difference in behavior of the amorphous and oriented films provides evidence for structure sensitivity in $Mg_3(VO_4)_2$ ODH catalysts. The (021) surfaces of the oriented films display far greater variations in surface composition during reduction/oxidation cycles than the surfaces of the amorphous films, which presumably consist of a thermodynamically weighted statistical mixture of various crystalline planes. One possible explanation for the structure sensitivity is that transport of oxygen vacancies from the surface to the bulk is slower at (021) surfaces than at other surfaces. As a result, the amorphous films are able to accommodate oxygen vacancies through diffusion into the bulk at vacancy concentrations that result in accommodation *via* V reduction and spreading on the (021) surface.

The most definitive demonstration of structure sensitivity would involve tests of the catalytic activity of the amorphous and oriented films. Extensive efforts were made to measure the ODH activity of the $Mg_3(VO_4)_2$ films in a flow reactor successfully used to test high surface area powdered propane ODH catalysts [7]. Unfortunately, the extremely low surface area of the films, coupled with a large void volume which promoted homogeneous reactions, prevented meaningful measurement of catalytic activity. Future experiments are planned to measure catalytic activity in a batch reactor where extended reaction times will allow measurable conversions to be achieved. These experiments should allow conclusive confirmation or refutation of the structure sensitivity of $Mg_3(VO_4)_2$ catalysts for ODH.

Conclusions

Tests of the behavior of $Mg_3(VO_4)_2$ films under reaction conditions approximating those typically found during propane ODH demonstrate the effects of oxygen vacancies and film surface structure on film reactivity. For (021) oriented films the presence of oxygen vacancies in the bulk decreases the rate at which surface vacancies, formed by reaction with propane, diffuse into the bulk. As a result surface oxygen vacancies are more likely to be accommodated by formation of reduced V at the surface, accompanied by spreading of a reduced V phase across the surface. This process appears to be at least partially reversible upon oxidation of the surface, resulting in reoxidation of V to the +5 state and reincorporation of V back into the bulk. Chemical behavior of the (021) surface is highly history dependent. Initial oxidation of the films tends to eliminate oxygen vacancies and decrease the likelihood that subsequent reduction will result in formation of the reduced V phase. Initial reduction of the films increases oxygen vacancy concentration, promoting formation of the reduced V phase and decreasing the

likelihood that subsequent oxidation will restore the initial state of the film. Fully oxidized films, containing few oxygen vacancies, display behavior that closely resembles that of $Mg_3(VO_4)_2$ powders, confirming that the films are good models for ODH catalysts.

Comparison of (021) oriented films with amorphous films deposited provides the first reported evidence for structure sensitivity in these materials. The amorphous films are far less likely to exhibit reduced V at the surface than the (021) oriented films. This difference may be attributed to higher rates of diffusion of oxygen vacancies from the surface into the bulk on the amorphous films.

Figure 1. XPS of the V2p and O 1s regions of a 200 nm $Mg_3(VO_4)_2$ film prepared with 2.5 sccm oxygen: a) as prepared film, b) treatment in 100 Torr propane for 1h at 773K, c) treatment in 100 Torr propane for 2h at 773K, d) reoxidation in 50 Torr oxygen at 673K for 1h.

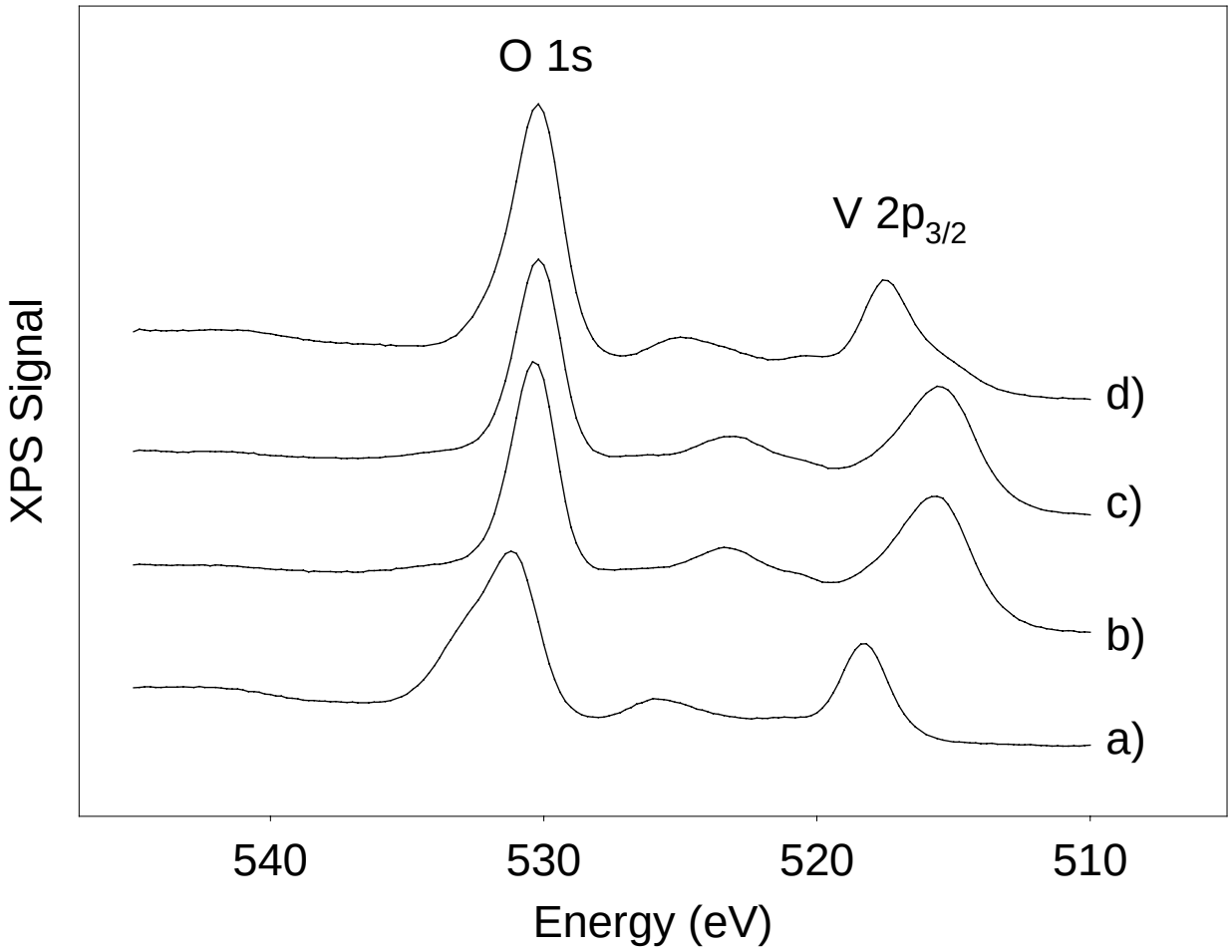

Figure 2. FTIR spectra of a 200 nm $Mg_3(VO_4)_2$ film prepared with 2.5 sccm oxygen: a) as prepared film, b) after treatment in 100 Torr propane for 2h at 773K, c) after reoxidation in 50 Torr oxygen at 673K for 1h. Shown for comparison in d) is the spectrum of a 200 nm film prepared in the absence of oxygen, which is known to contain $Mg_3V_2O_6$ (see chapter 2).

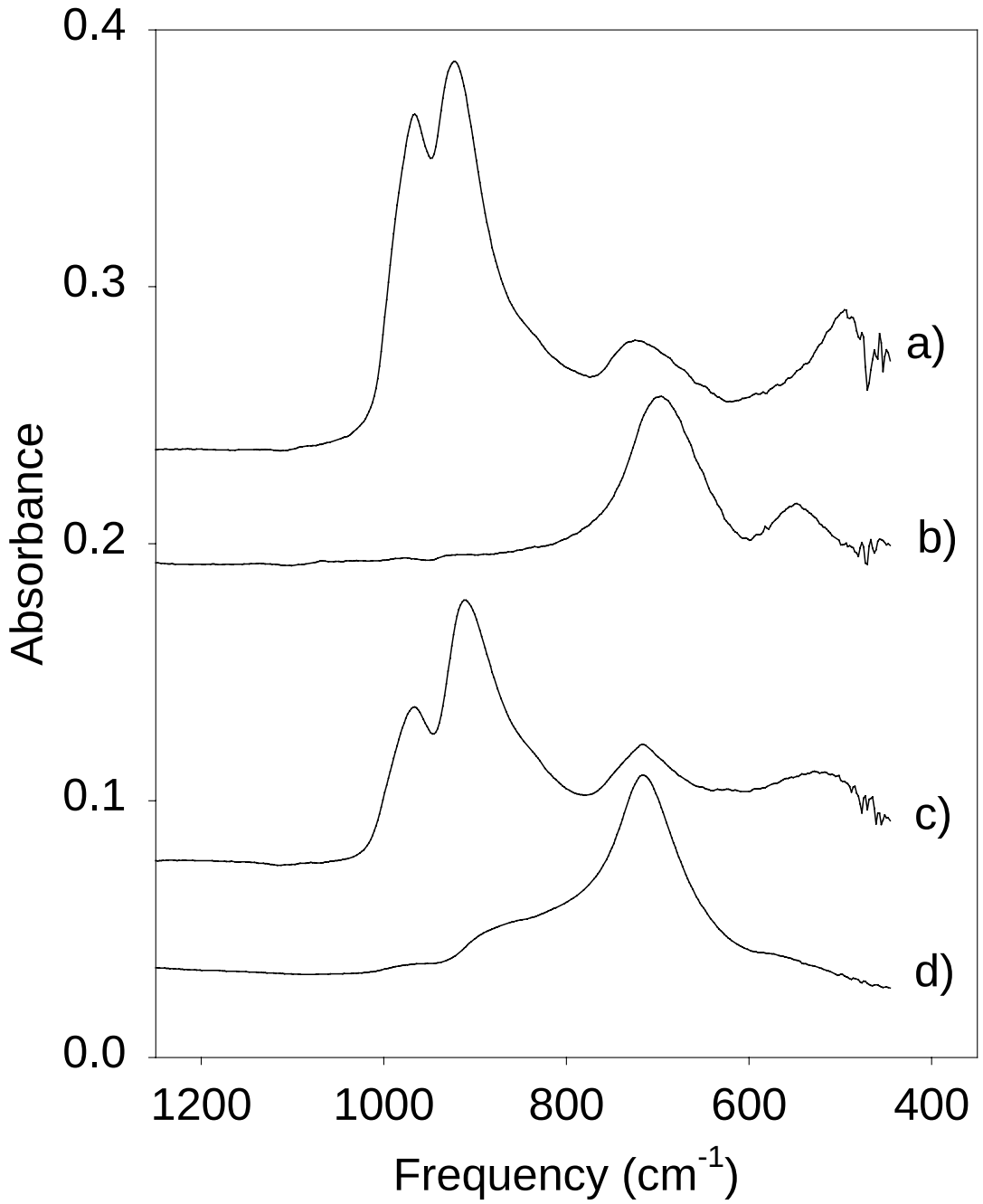

Figure 3. XPS of MgVO-o(2.5) film following cyclic reduction/oxidation treatments: a) as prepared film; b) 100 Torr propane, 673K, 1h; c) 50 Torr oxygen, 673K, 0.5h; d) 100 Torr propane, 673K, 1h; e). 50 Torr oxygen, 673K, 0.5h.

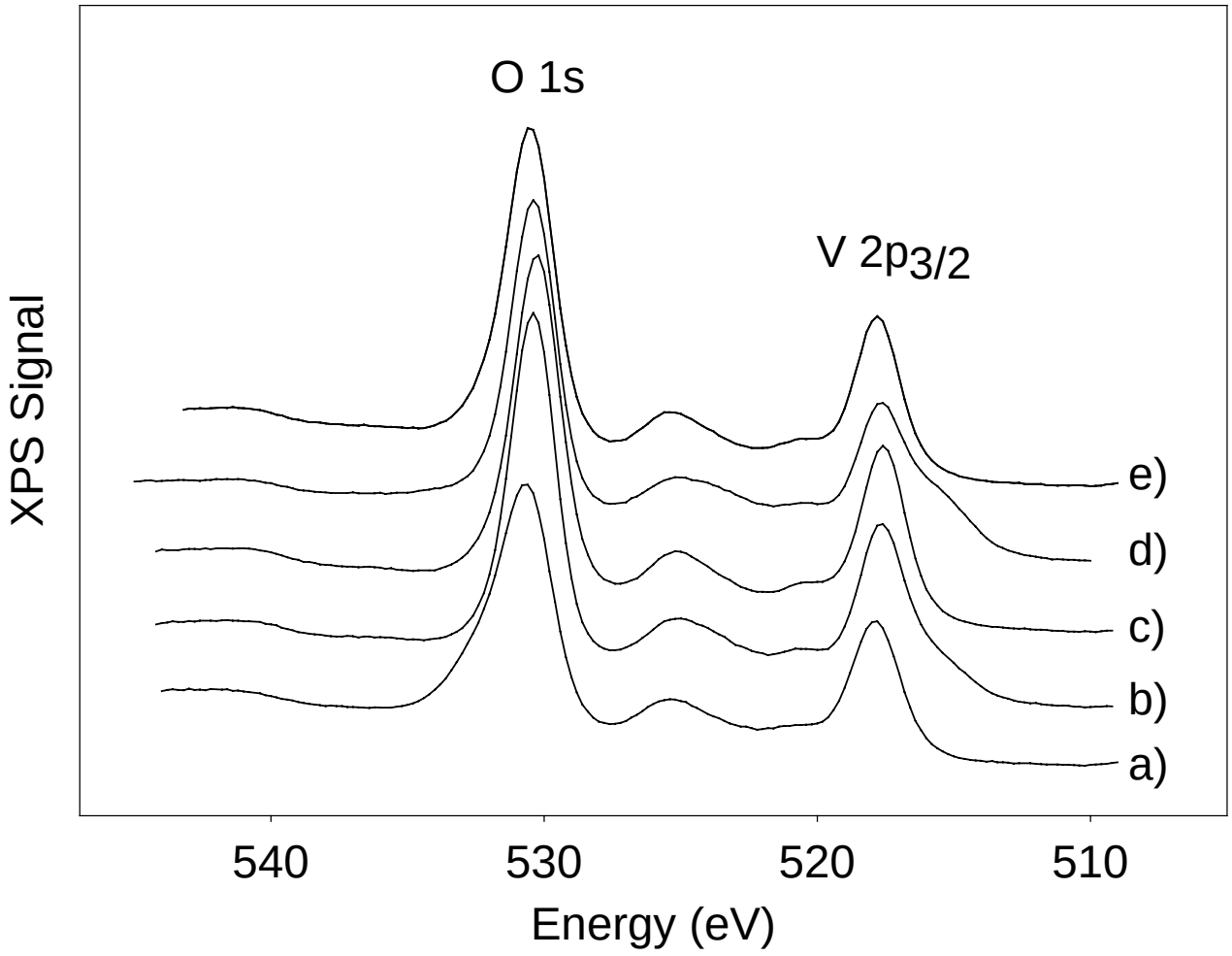

Figure 4. Effect of reactive treatments on the surface composition of the MgVO-o(5.0) film. Propane/oxygen treatments were performed for 1h in the presence of 50 Torr O_2 and 100 Torr propane. Oxygen treatments were performed under 50 Torr O_2, while propane treatments were performed under 100 Torr propane. Treatment temperatures are indicated in the figure. Circles: treatment in propane oxygen mixtures followed by oxidation/reduction cycles; triangles: oxidation/reduction cycles beginning with oxidation; squares: oxidation/reduction cycles beginning with reduction.

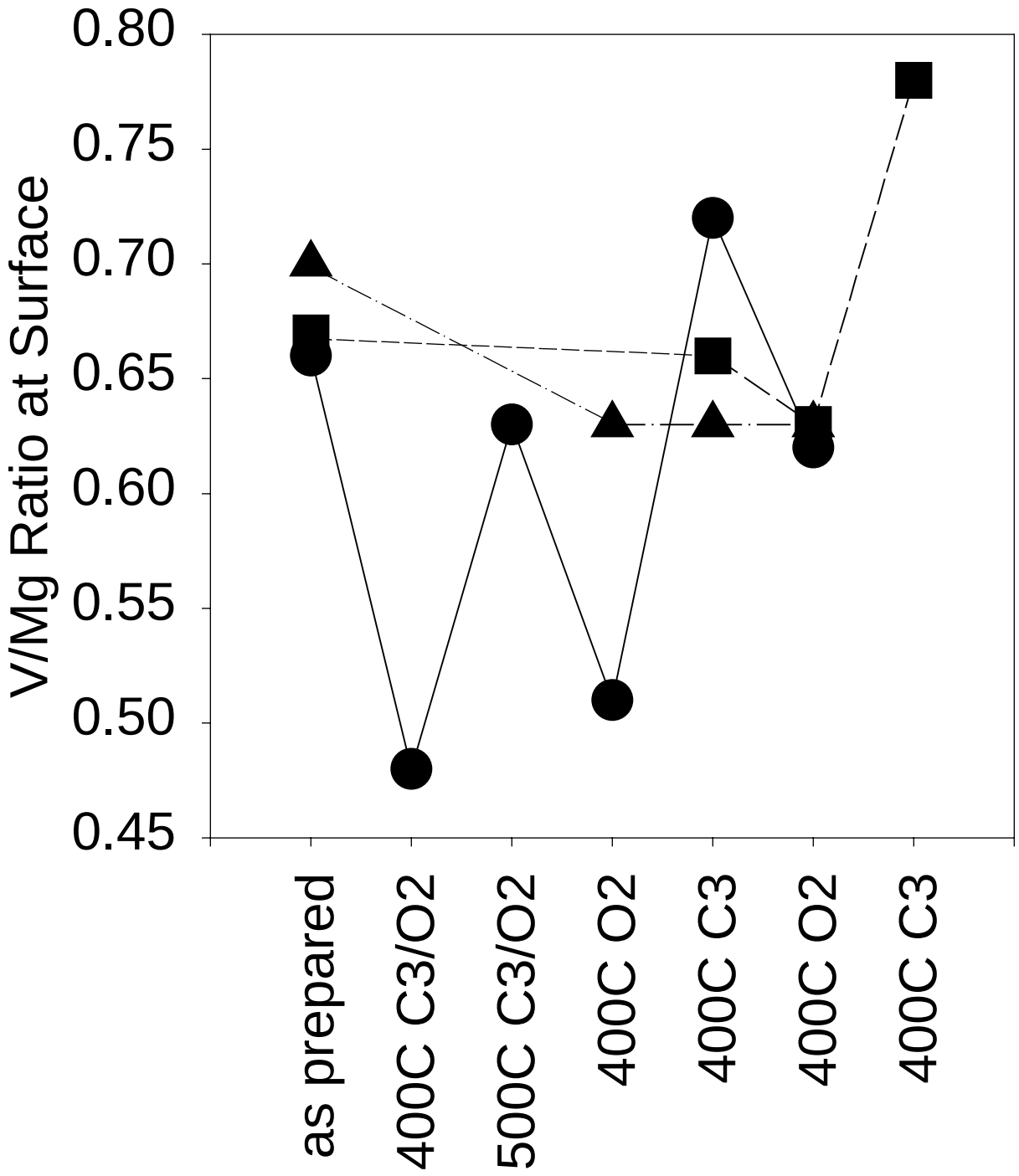

Figure 5. Effect of reduction/oxidation cycles on the surface composition of oriented films as a function of oxygen flow rate during deposition. Reduction treatments are at 673K under 100 Torr propane for 1h, while oxidation treatments are at 673K under 50 Torr oxygen for 0.5h. Initial treatment is reduction.

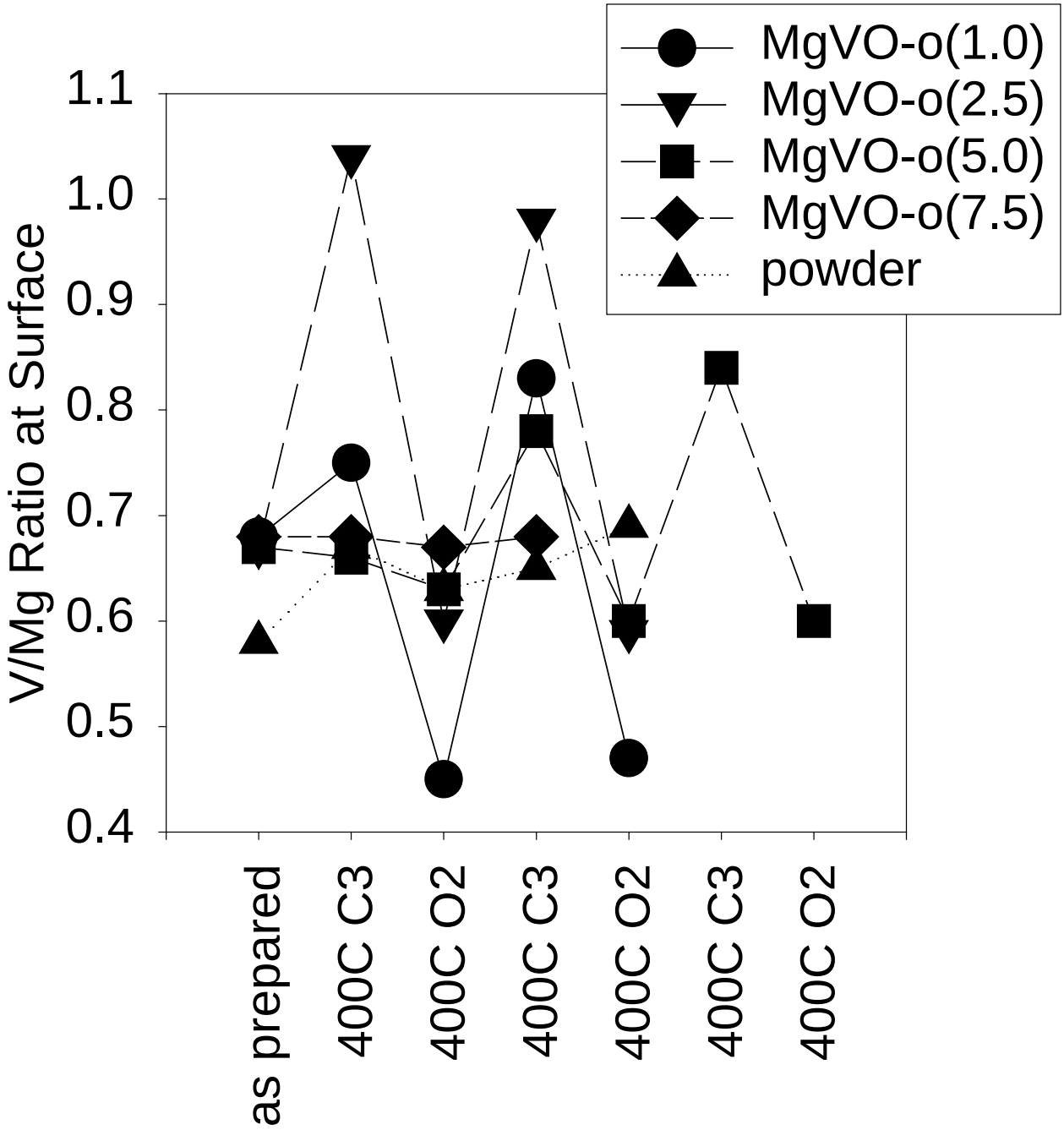

Figure 6. Effect of oxidation/reduction cycles on the surface composition of oriented films as a function of oxygen flow rate during deposition. Reduction treatments are at 673K under 100 Torr propane for 1h, while oxidation treatments are at 673K under 50 Torr oxygen for 0.5h. Initial treatment is oxidation.

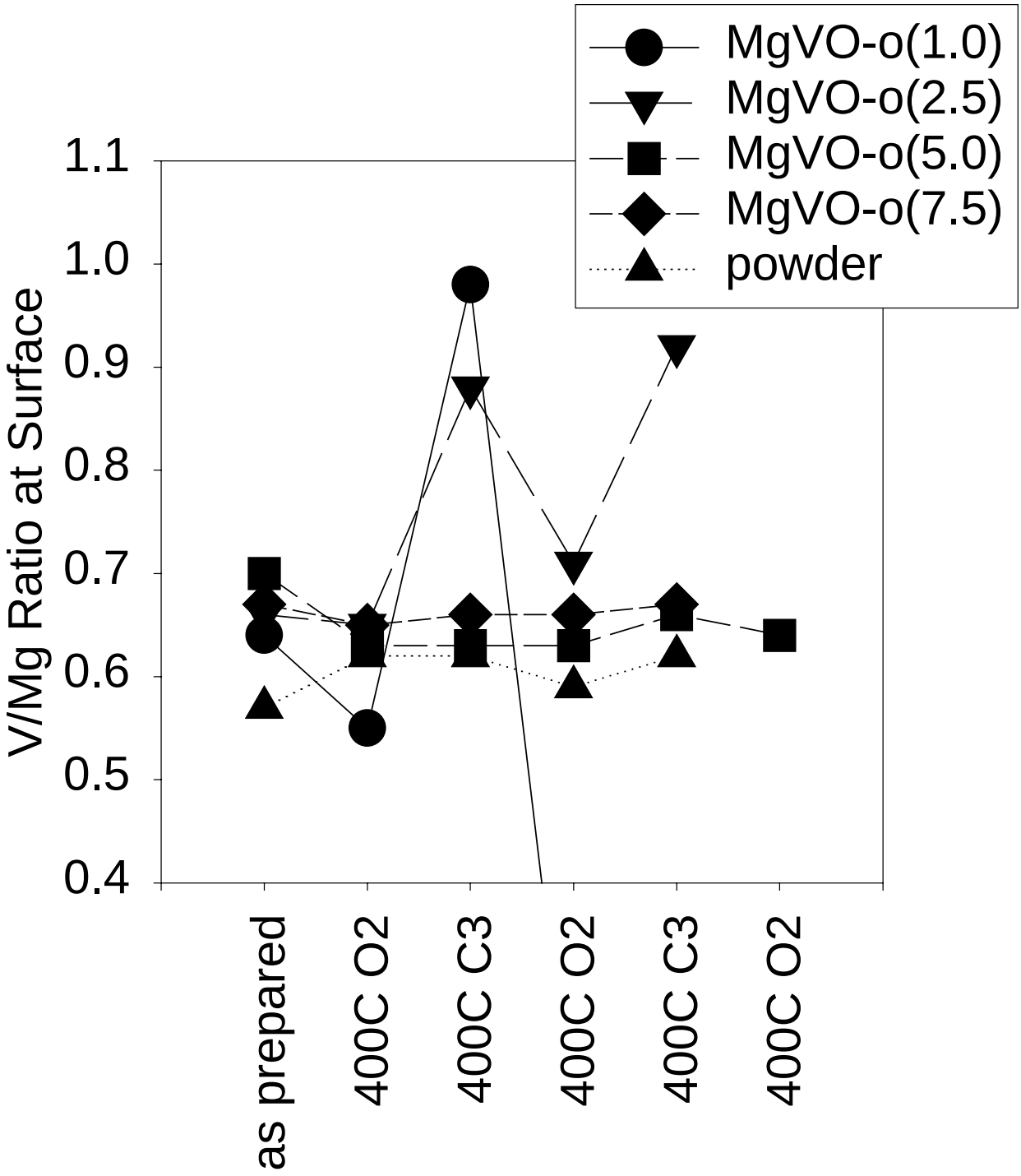

Figure 7. Comparison of oriented and amorphous film surface composition during reduction/oxidation cycles. Reduction treatments are at 673K under 100 Torr propane for 1h, while oxidation treatments are at 673K under 50 Torr oxygen for 0.5h. Initial treatment is reduction.

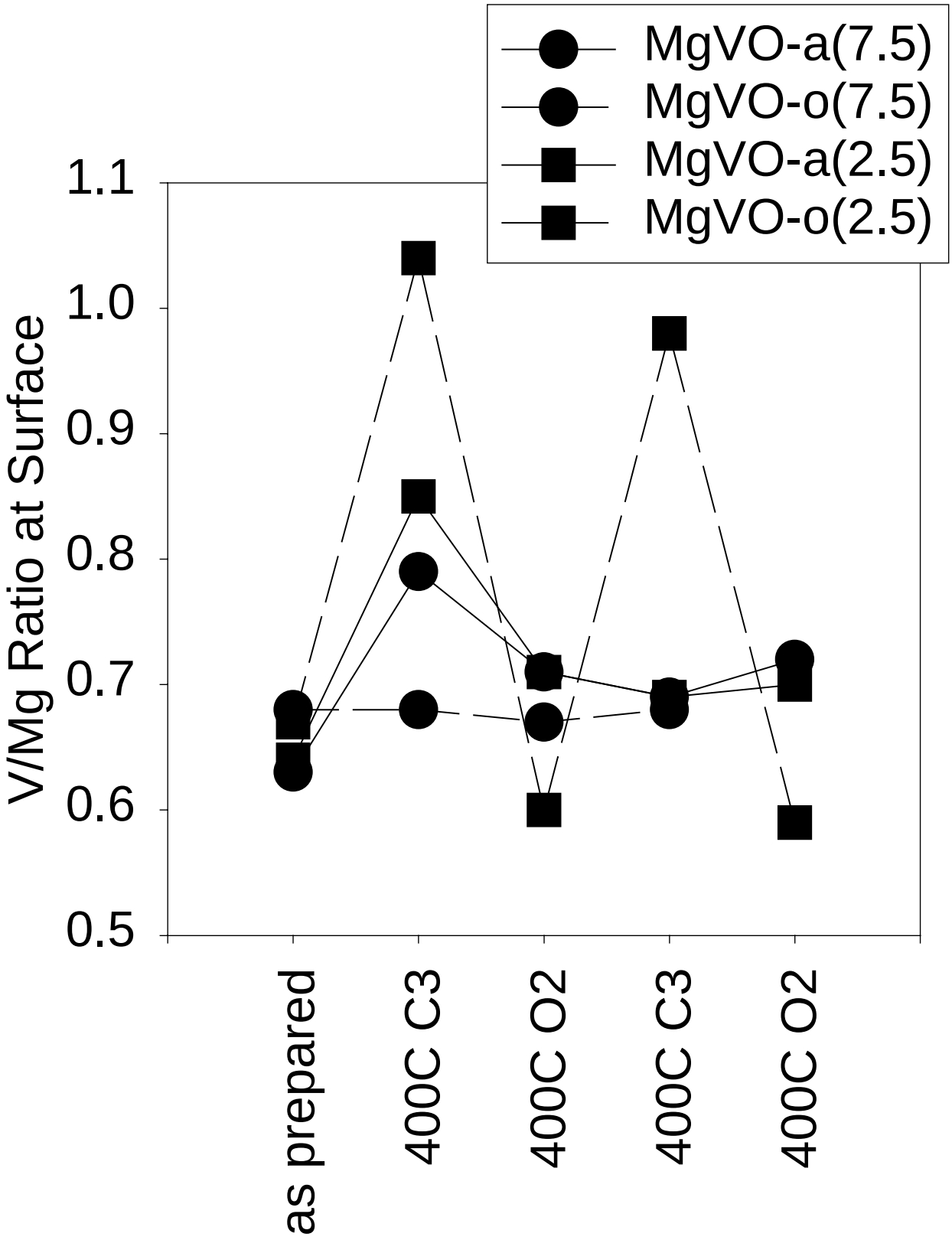

Figure 8. Comparison of oriented and amorphous film surface composition during oxidation/reduction cycles. Reduction treatments are at 673K under 100 Torr propane for 1h, while oxidation treatments are at 673K under 50 Torr oxygen for 0.5h. Initial treatment is oxidation.

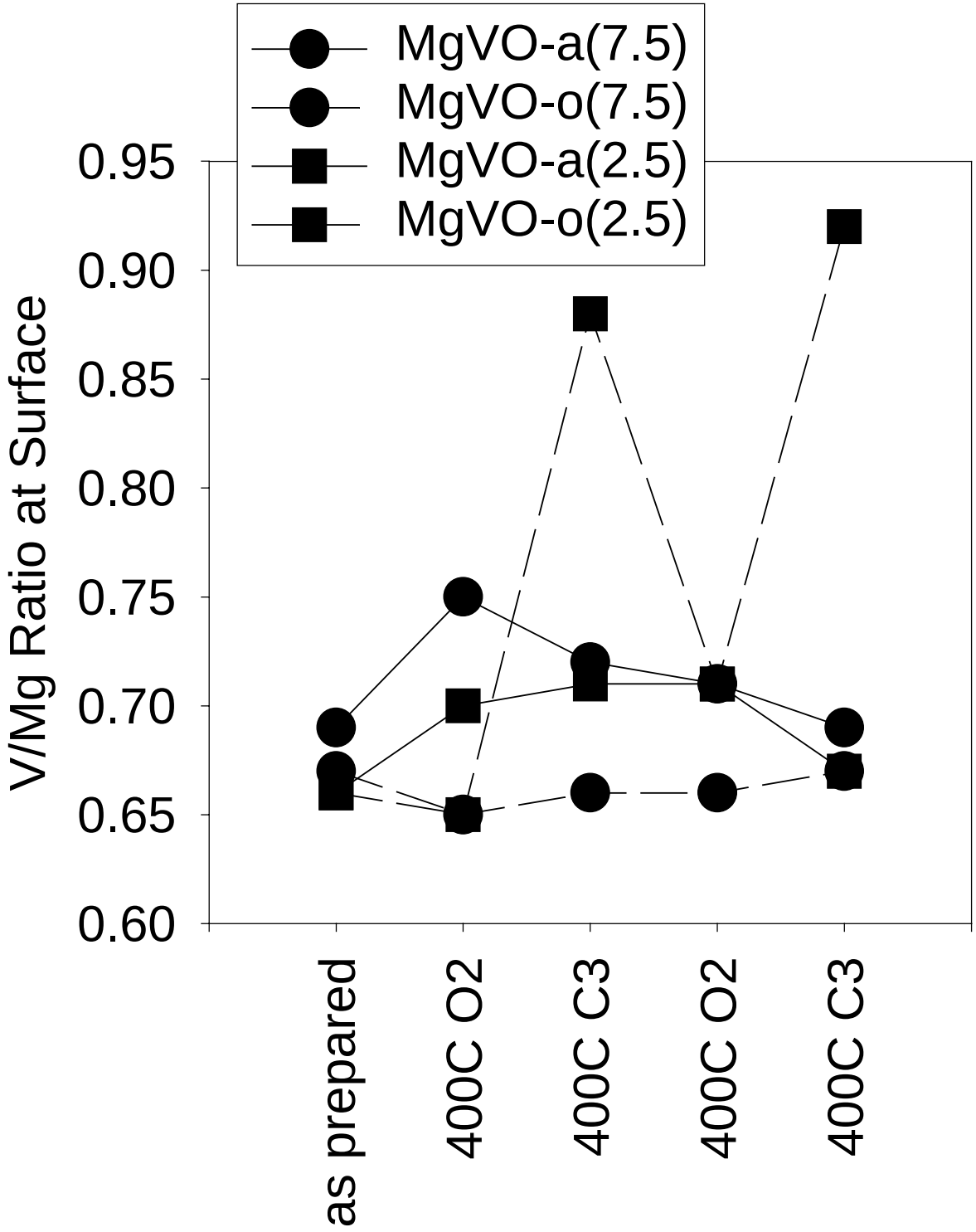

Chapter 3 Reference

1 H. H. Kung, Adv. Catal., **40** (1994) 1.

2 D. Siew Hew Sam, V. Soenen, and J. C. Volta, J. Catal., **123** (1990) 417.

3 X. Gao, P. Ruiz, X. Guo, and B. Delmon, J. Catal., **148** (1994) 56.

4 S. R. G. Carrazán, C. Peres, J. P. Bernard, M. Ruwet, P. Ruiz, and B. Delmon, J. Catal., **158** (1996) 452.

5 X. Wang, H. Zhang, W. Sinkler, K. R. Poeppelmeier, and L. D. Marks, J. Alloys Cmpds., **270** (1998) 88.

6 Ph. Courty, H. Ajot, Ch. Marcilly, and B. Delmon, Powder Technol., **7** (1973) 21.

7 J. E. Miller, N. B. Jackson, L. Evans, A. G. Sault, and M. M. Gonzales, Catal. Lett., **58** (1999) 147.

8 C. D. Wagner, L. E. Davis, M. V. Zeller, J. A. Taylor, R. M. Raymond, and L. H. Gale, Surf. Interface Anal., **3** (1981) 211.

9 PDF card 19-0778, JCPDS – International Center for Diffraction Data, Newtown Square, PA.

10 A. Burrows, C. J. Kiely, J. Perregaard, P. E. Højlund-Nielsen, G. Vorbeck, J. J. Calvino, and C. López-Cartes, Catal. Lett., **57** (1999) 121.

11 S. A. Stevenson, J. A. Dumesic, R. T. K. Baker, and E. Ruckenstein, "Metal-Support Interactions in Catalysis, Sintering, and Redispersion," (Von Nostrand Reinhold Co., New York, 1987).

12 A. Patazidis, A. Burrows, C. J. Kiely, and C. Miradatos, J. Catal., **177** (1998) 325.

DISTRIBUTION:

1	MS 0188	LDRD Office, 4001
1	MS 1411	Mark A. Rodriguez, 1822
1	MS 1411	Ralph G. Tissot, Jr., 1822
1	MS 0886	Nancy B. Jackson, 1841
2	MS 1349	James E. Miller, 1841
2	MS 1349	Jason E. Mudd, 1841
10	MS 1349	Allen G. Sault, 1841
5	MS 1349	Heidi Ruffner, 1846
1	MS 9018	Central Technical Files, 8945-1
2	MS 0899	Technical Library, 9616
1	MS 0612	Review & Approvale Desk, 9612 For DOE/OSTI